

**Coupled ice
sheet–climate
modeling**

F. A. Ziemer et al.

This discussion paper is/has been under review for the journal Climate of the Past (CP).
Please refer to the corresponding final paper in CP if available.

Coupled ice sheet–climate modeling under glacial and pre-industrial boundary conditions

F. A. Ziemer^{1,2,*}, C. B. Rodehacke^{1,}, and U. Mikolajewicz¹**

¹Max Planck Institute for Meteorology, Bundesstr. 53, 20146 Hamburg, Germany

²International Max Planck Research School on Earth System Modelling (IMPRS),
Bundesstr. 53, 20146 Hamburg, Germany

*now at: Geophysical Institute, University of Alaska, Fairbanks, USA

**now at: Danish Meteorological Institute, Copenhagen, Denmark

Received: 8 January 2014 – Accepted: 23 January 2014 – Published: 11 February 2014

Correspondence to: F. A. Ziemer (florian.ziemer@mpimet.mpg.de)

Published by Copernicus Publications on behalf of the European Geosciences Union.

Title Page

Abstract

Introduction

Conclusions

References

Tables

Figures



Back

Close

Full Screen / Esc

Printer-friendly Version

Interactive Discussion



Abstract

We studied the climate of the last glacial maximum (LGM) in a set of coupled ice sheet–climate model experiments. They are based on the standard Paleoclimate Modelling Intercomparison Project Phase 2 (PMIP-2) experiments and extend the PMIP-2 (and PMIP-3) protocol by explicitly modeling the ice sheets. This adds a new layer of complexity and yields a set of ice sheets and climate that interact and are consistent with each other. We studied the behavior of the ice sheets and the climate system and compared our results to proxy data.

The setup consists of the atmosphere-ocean-vegetation general circulation model ECHAM5/MPIOM/LPJ bidirectionally coupled with the Parallel Ice Sheet Model (PISM). We validated the setup by comparing the LGM experiment results with proxy data and by performing a pre-industrial control run. In both cases, the results agree reasonably well with reconstructions and observations. This shows that the model system adequately represents large, non-linear climate perturbations.

Under LGM boundary conditions, the surface air temperature decreases by 3.5 K, and the precipitation north of 45°N by 0.12 myr⁻¹ (–18%) compared to the pre-industrial conditions. The North Atlantic Deep Water cell strengthens from 17.0 to 22.1 Sv (1 Sv = 10⁶ m³ s⁻¹) and the deep water formation shifts from the Labrador and GIN Seas to southeast of Iceland. Under LGM boundary conditions, different ice sheet configurations imply different locations of deep water formation. The major ice streams form in topographic troughs. In large parts, the modeled ice stream locations agree with sedimentary seafloor deposits. Most ice streams show recurring surges. The Hudson Strait Ice Stream surges with an ice volume equivalent to about 5 m sea level and a recurrence interval of about 7000 yr.

CPD

10, 563–624, 2014

Coupled ice sheet–climate modeling

F. A. Ziemeň et al.

Title Page

Abstract

Introduction

Conclusions

References

Tables

Figures



Back

Close

Full Screen / Esc

Printer-friendly Version

Interactive Discussion



1 Introduction

The understanding of past climates is a major challenge. By modeling past climates which differ strongly from the present-day climate, we study documented, non-linear climate changes. With these studies, we improve the understanding of the climate system (Valdes, 2011; Braconnot et al., 2012).

The last period with a climate substantially different from the present-day climate was the last glacial. It is very recent from a geological perspective, therefore the proxy coverage is comparatively good. The climate differences between the last glacial and the present mainly stem from the reduced greenhouse gas content of the atmosphere and from the massive ice sheets covering the continents of the Northern Hemisphere (Rind, 1987; Kim, 2004; Abe-Ouchi et al., 2007; Pausata et al., 2011). The ice sheets were at their maximum volume about 21 000 yr ago, during the last glacial maximum (LGM) (e.g. Clark et al., 2009). In contrast to the following deglaciation that is a transient process, the LGM climate is commonly assumed to be in a reasonably steady state and it is common practice (e.g. in the Paleoclimate Modelling Intercomparison Project, PMIP) to perform steady-state experiments under LGM boundary conditions.

Previous atmosphere-ocean general circulation model (AOGCM) studies of the LGM climate, especially the PMIP experiments, have relied on prescribing the ice sheets from reconstructions (Braconnot et al., 2007, 2011, 2012). While the original PMIP experiments prescribed sea surface temperatures (SSTs) or oceanic heat transports, and PMIP-2 added the full ocean models to the complexity, interactive ice sheets are still missing, even in PMIP-3. This can result in climate and ice sheets not being consistent with each other. To obtain ice sheets that are consistent with the modeled climate, it is essential to overcome this method and model the ice sheets interactively. We took exactly this step. We extended the PMIP-2 setup by an interactively coupled ice sheet model and studied the climate as well as the ice sheets in this self-consistent system with its increased complexity. By comparing the modeled ice sheets with reconstructions, we can critically assess our model system.

CPD

10, 563–624, 2014

Coupled ice sheet–climate modeling

F. A. Ziemer et al.

Title Page

Abstract

Introduction

Conclusions

References

Tables

Figures



Back

Close

Full Screen / Esc

Printer-friendly Version

Interactive Discussion



**Coupled ice
sheet–climate
modeling**

F. A. Ziemeň et al.

[Title Page](#)[Abstract](#)[Introduction](#)[Conclusions](#)[References](#)[Tables](#)[Figures](#)[Back](#)[Close](#)[Full Screen / Esc](#)[Printer-friendly Version](#)[Interactive Discussion](#)

An interactively coupled ice sheet–climate model opens the possibility of studying the interactions between ice sheets and the climate system. In the light of the recently observed changes in the ice sheets and their potential impact on future sea level rise, such studies become increasingly relevant for predicting future climate change. The large ice masses and the possibility of comparing the model results to proxy data make the LGM an ideally suited time period for studying ice–climate interactions.

The main challenge in coupled ice sheet–climate modeling is that the time scales of ice sheets are much longer than the typical time scales of the atmosphere–ocean system and most of the snowfall and melt occurs in a narrow band along the ice sheet margin. In principle, the margin zone calls for high-resolution modeling, while the long time scales prohibit this. The discrepancy between the need for high resolution modeling and long time spans leads to a variety of strategies (see the review by Pollard, 2010).

At the fast and simple end of the model spectrum, fixed climate maps or analytical expressions are scaled by the use of a time series, either from an energy balance model or from ice core data. In the earlier times, these models were used to study one glacial cycle (e.g., Pollard, 1982; Greve, 1997; Tarasov and Peltier, 1997). Advances in computing power now make it possible to model the evolution of the ice sheets over millions of years with such models (Pollard and DeConto, 2009). Tarasov et al. (2012) performed multiple experiments covering the last glacial. They chose the experiments that agreed best with the proxy data and created a deglacial ice sheet chronology that is consistent with proxy data as well as with ice physics.

Zweck and Huybrechts (2003) forced an ice sheet model by interpolating between modeled climate states for LGM and modern boundary conditions using Greenland ice core data as weighting coefficients. Charbit et al. (2007) compared the effect of different AGCMs on the same ice sheet model using a similar approach. Abe-Ouchi et al. (2007, 2013) combined output from multiple experiments performed with the same climate model to account for changes in greenhouse gases, orbital parameters, and ice sheets separately.

Coupled ice sheet–climate modeling

F. A. Ziemer et al.

[Title Page](#)[Abstract](#)[Introduction](#)[Conclusions](#)[References](#)[Tables](#)[Figures](#)[Back](#)[Close](#)[Full Screen / Esc](#)[Printer-friendly Version](#)[Interactive Discussion](#)

Another approach uses earth system models of intermediate complexity (EMICs) and optionally downscales the fields for the ice sheet model in an intermediate energy balance model or energy-moisture balance model. Such models have been used to study processes like Heinrich events (Calov et al., 2002) and glacial inception (Wang and Mysak, 2002; Calov et al., 2005), or more recently, full glacial cycles (Bonelli et al., 2009; Ganopolski et al., 2010; Ganopolski and Calov, 2011).

The most expensive approaches use coupled AOGCM–ice sheet model (ISM) systems. While the EMIC or energy balance model based methods can cover long time spans with reasonable effort, they strongly simplify the climate system. In contrast, AOGCMs suffer from high computational costs but provide a detailed representation of the climate system. To bridge the long time spans, most research groups couple the models asynchronously. In this method, the climate model is run for a period of one to fifty years, and then the climate is used to drive the ice sheet for a substantially longer period. The resulting ice sheet is fed back into the climate model and the cycle is started over (Pollard et al., 1990; Ridley et al., 2005; Mikolajewicz et al., 2007a; Gregory et al., 2012).

Several previous AOGCM–ISM studies investigated the future development of the Greenland ice sheet and its impact on the Atlantic meridional overturning circulation (AMOC). Early studies by Huybrechts et al. (2002) and Fichefet et al. (2003) only fed back the fresh water fluxes but kept the Greenland topography constant in the AOGCM. The first study with a full bidirectional coupling between an AOGCM and an ISM was published by Ridley et al. (2005). It was followed by studies that also include the Antarctic Ice Sheet (Mikolajewicz et al., 2007a, b; Vizcaíno et al., 2008, 2010). The experiments presented in Mikolajewicz et al. (2007b) and Vizcaíno et al. (2010) were the first atmosphere–ocean–vegetation general circulation model (AOVGCM)–ISM studies to use an energy balance model for the surface mass balance of the ice sheet and the first to operate without anomaly maps. This improved the physical representation of the coupling. A recent study by Gregory et al. (2012) used the AOGCM FAMOUS, a fast

version of HADCM3 in combination with the ice sheet model GLIMMER to study the last glacial inception. None of the published studies address LGM conditions.

We have coupled a coarse-resolution setup of the AOVGCM ECHAM5/MPIOM/LPJ interactively with a state-of-the-art ISM, the modified Parallel Ice Sheet Model (mPISM).

The coupling is performed bidirectionally, and without flux corrections nor anomaly methods. With this model system, we performed experiments under pre-industrial as well as fixed LGM boundary conditions. The only factors we prescribed were the greenhouse gas concentrations, the orbitals and the shapes of the continents. We let the models evolve freely sufficiently long to be largely independent of the initial state. We study the behavior of the climate system and compare the model results to observations and proxy-data.

This study has a strong technical component in developing a coupled model system and tests the applicability of the coupled system to the pre-industrial, and glacial climates. We describe the models, the necessary modifications, the coupling as well as the setups in Sect. 2, analyze the mean states of the experiments in Sect. 3, and summarize the main findings and draw the conclusions in Sect. 4.

2 Model description and setups

The AOVGCM has been applied before coupled to the ISM SICOPOLIS for studies of the future evolution of the Greenland and Antarctic ice sheets (Mikolajewicz et al., 2007b; Vizcaíno et al., 2010). For this study, we have switched to Parallel Ice Sheet Model (PISM), and changed various aspects of the coupling. The models and the coupling will be described in the following.

2.1 ECHAM5/MPIOM/LPJ

The atmospheric component of the coupled model is ECHAM5 (Roeckner et al., 2003), a spectral atmosphere general circulation model. For long-term simulations, the

CPD

10, 563–624, 2014

Coupled ice sheet–climate modeling

F. A. Ziemer et al.

Title Page

Abstract

Introduction

Conclusions

References

Tables

Figures

⏪

⏩

◀

▶

Back

Close

Full Screen / Esc

Printer-friendly Version

Interactive Discussion



**Coupled ice
sheet–climate
modeling**

F. A. Ziemeň et al.

Title Page

Abstract

Introduction

Conclusions

References

Tables

Figures

⏪

⏩

◀

▶

Back

Close

Full Screen / Esc

Printer-friendly Version

Interactive Discussion



triangular spectral truncation at wavenumber 31 (T31, $\sim 3.75^\circ$) in combination with 19 vertical hybrid- σ -levels reaching up to 10hPa is a compromise between computational demand and accuracy. This setup is therefore employed in all experiments described in the following. The land hydrology scheme (HD model, Hagemann and Dümenil, 1998; Hagemann and Gates, 2003) operates on a 0.5° grid. For the HD model, we use the present-day routing directions in combination with the LGM land-sea-mask. The land surface properties are modeled using the Lund-Potsdam-Jena (LPJ) vegetation model (Sitch et al., 2003). Its use in combination with ECHAM is described in Schurgers et al. (2007) and Mikolajewicz et al. (2007a).

MPIOM (Marsland et al., 2003) is a primitive equation ocean model operating on a curvilinear grid with variable resolution. In the setup employed in the following, the grid has two poles, located over Greenland and Antarctica, and a nominal resolution of 3° . This results in an increased resolution in the deep water formation areas, and a relatively coarse resolution in the equatorial areas.

The atmosphere and ocean are coupled using the OASIS coupler (Valcke et al., 2004). The performance of a higher-resolution version of the coupled AOGCM is described in Jungclaus et al. (2006). Results of the T31-setup in the framework of the PMIP-2 can be found in the PMIP-2 database at <http://pmip2.lsce.ipsl.fr>.

2.2 mPISM

The modified Parallel Ice Sheet Model is based on PISM version 0.3 from the University of Alaska, Fairbanks (Bueler and Brown, 2009; the PISM authors, 2013). PISM uses the Shallow Ice Approximation (SIA) and the Shallow Shelf Approximation (SSA) to compute flow velocities. It uses an enthalpy method to handle polythermal ice (Aschwanden et al., 2012). Details about the model can be found in the literature given above. Several aspects of the model needed to be changed for the coupling to the climate model and for obtaining pulsating ice streams. In the following, we describe the modifications of the PISM physics. For the technical changes see Ziemeň (2013). We use the term PISM 0.3 when referring to the base version, mPISM when referring to the modified

version, and PISM when referring to aspects of the base version that also apply to the modified version. PISM-PIK (Winkelmann et al., 2011) is a branch of PISM that is developed at the Potsdam Institute for Climate Impact Research (PIK).

Following Calov et al. (2002), we use a linear sliding law that allows sliding if there is basal water and deformable sediment available to lubricate the ice sheet. The availability of the sediment is based on the dataset from Laske and Masters (1997) with a cutoff value of 5 cm and is marked in Fig. 1. The availability of basal water is a prognostic quantity of PISM. We spread out half of a grid cell's heat flux from basal friction on the cells eight neighbors. This slightly heats the grid cells adjacent to an ice stream.

We separate the basal water into a small locally bound fraction and an advectable fraction that we advect with the basal ice velocity and apply the same upwind scheme as used for ice and enthalpy transport. The locally bound fraction controls the stiffness of the basal till and thereby the sliding behavior.

For the bedrock deformation, we use an Local Lithosphere Relaxed Asthenosphere (LLRA) model (e.g. Le Meur and Huybrechts, 1996) with a rebound timescale of 3 kyr. We dynamically compute the change in sea level that is caused by the ice sheets and use it to adjust the sea level in the ice sheet model and in the climate model.

Our setup uses a Cartesian coordinate system that is a Polar Stereographic projection of the Northern Hemisphere, covers all areas north of 36.7° N and reaches south to 19.1° N in the corners. This grid covers all Northern Hemisphere regions we can possibly expect to grow large-scale ice sheets under glacial conditions (including the Himalayans). The resolution is 20 km in both directions (625 × 625 grid cells). Outside of the the modified Parallel Ice Sheet Model domain, we use the ICE-5G (Peltier, 2004) topography matching the time slice of interest as in PMIP-2.

2.3 The coupling from the climate to the ice sheet

The coupling scheme between ECHAM5, MPIOM and mPISM computes the ice sheet mass balance and surface temperature from the ECHAM5 and MPIOM output and

CPD

10, 563–624, 2014

Coupled ice sheet–climate modeling

F. A. Ziemer et al.

Title Page

Abstract

Introduction

Conclusions

References

Tables

Figures



Back

Close

Full Screen / Esc

Printer-friendly Version

Interactive Discussion



transfers surface topography, glacier mask and mass fluxes from mPISM back to ECHAM5 and MPIOM. We will now lay out the path from the climate model to mPISM.

To compute the mass balance for the ice sheet, we have to use a high spatial resolution that resolves the temperature distribution at the ice sheet margins. We use the 20 km grid of mPISM for the mass balance calculations. To save computational time, we compute monthly averages of the atmospheric quantities and annual averages of the ocean variables before regridding them to the ice sheet model grid. These regridded high-resolution fields are used in the ice sheet model to determine the mass balance. The scheme we use to process temperatures and precipitation from ECHAM5 for the use in mPISM is based on the standard scheme employed in SICOPOLIS (Calov, 1994), which stems from Braithwaite and Olesen (1989).

To account for surface elevation differences between the two models, we correct the temperatures using a lapse rate of -5 K km^{-1} as suggested by Abe-Ouchi et al. (2007). We use the height corrected monthly mean temperatures to partition the precipitation into solid and liquid fractions using a linear transition between -10 and $+7^\circ\text{C}$ as in Mariat (1994). The solid fraction is used as accumulation, the liquid fraction is discarded immediately as runoff. To account for the reduced precipitation at high altitudes, we apply a height desertification parametrization as in Budd and Smith (1979) at heights above 2000 m.

$$P = P_{\text{solid}} \exp(-\lambda (\max(h_{\text{ISM}}, 2000 \text{ m}) - \max(h_{\text{GCM}}, 2000 \text{ m}))), \quad (1)$$

where h_{ISM} is the surface height in the modified Parallel Ice Sheet Model, h_{GCM} is the surface height in the climate model, and $\lambda = \log(2)/1000 \text{ m}$.

We use temperatures and precipitation in a Positive Degree Day (PDD) model to determine the surface mass balance. As an extension of Fausto et al. (2011), we compute monthly temperature standard deviation maps from the 6 hourly climate model output and use them in mPISM to better represent the temperature variability. This is a compromise between computing the PDDs from the full 6 hourly temperature data on the highly resolved ice grid (which would be more computationally demanding) and

Coupled ice sheet–climate modeling

F. A. Ziemer et al.

Title Page

Abstract

Introduction

Conclusions

References

Tables

Figures

◀

▶

◀

▶

Back

Close

Full Screen / Esc

Printer-friendly Version

Interactive Discussion



Coupled ice sheet–climate modeling

F. A. Ziemer et al.

Title Page

Abstract

Introduction

Conclusions

References

Tables

Figures



Back

Close

Full Screen / Esc

Printer-friendly Version

Interactive Discussion



the standard approach of prescribing a fixed standard deviation in the full model domain. The PDD scheme employs the Calov-Greve integral method (Calov and Greve, 2005) to compute PDDs from monthly mean temperatures and standard deviations. Then, from these PDD, and the snow accumulation, the actual mass balance is computed using a standard PDD scheme (Reeh, 1991). We chose a snow melt rate of $m_{\text{snow}} = 3.2 \text{ mm K}^{-1} \text{ day}^{-1}$, an ice melt rate of $m_{\text{ice}} = 12.9 \text{ mm K}^{-1} \text{ day}^{-1}$ and allow up to 60% of the melt to refreeze in the snowpack.

For the basal ice shelf melt (or growth), we use the three equation scheme described in Holland and Jenkins (1999). This scheme computes the ice shelf basal mass balance and properties of a thin boundary layer from ocean salinity and temperature as well as the ice shelf basal temperature gradient. We force this model with the annual mean temperature and salinity averaged over the top 12 layers (203 m) from the ocean model.

We employ a simple calving scheme that operates on a grid cell and its eight neighbors. If less than three of the nine cells have an ice thickness above 200 m, and the relaxed bedrock topography is below sea level, then the ice is calved. This allows shelves to dynamically grow and retreat, and prevents one grid cell wide ice tongues.

2.4 The coupling from the ice sheet to the climate

In the following, we describe how the output fields from mPISM are fed back into ECHAM5 and MPIOM. We first detail on the surface orography, then on the glacier mask, and finally on the mass fluxes.

The orography is fed back into ECHAM5 via the geoid surface potential and the gravity wave drag parametrization. For the areas outside of the mPISM domain, the mPISM surface field is combined with a background map. The combined map is adjusted for sea level changes from the ice sheet. To keep the subgrid scale orography consistent, the background map is smoothed with respect to the standard topography map used for ECHAM5, so it matches the roughness of the ice-free areas of the remapped mPISM topography. Since this smoother surface would significantly change climate in comparison to the standard model setup, we upscale the subgrid surface slopes by a factor

of two. Furthermore, we decrease the resolution-dependent threshold for activating the gravity wave drag parametrization in ECHAM5 from 400m to 300m peak – mean elevation, so the gravity wave drag parametrization is active in about the same grid cells as in the original setup.

All ice sheet model grid cells with an ice thickness above 10m are treated as glaciated. We use conservative area remapping to interpolate the glacier mask to the ECHAM5 grid. ECHAM5 treats all grid cells with a fractional glacier mask value above 0.5 as fully glaciated. We modified the ECHAM5 albedo scheme, such that the albedo is computed based on a fractional glacier cover with a background albedo of 0.25 for the non-glaciated parts of the grid cell. For those grid cells that have a glacier fraction below 0.5 and are thus considered as non-glaciated, we reduce the forest (tree cover) fraction by the glacier fraction ($\text{forest}^{\text{new}}$) and compute a new background albedo α^{new} that represents the effects of the albedo of the glaciated parts:

$$\text{forest}^{\text{new}} = (1 - \text{glacier}) \text{forest}; \quad \alpha^{\text{new}} = \alpha_{\text{lpj}} (1 - \text{glacier}) + \alpha_{\text{glacier}} \text{glacier}, \quad (2)$$

where forest is the forest fraction computed by LPJ, glacier the glacier fraction from the remapped the mPISM output, α_{lpj} the background albedo calculated from the vegetation model, and α_{glacier} a background albedo for melting glacier ice (0.5). The reduction of the forest fraction is important because it reduces the snow-masking effect in the albedo calculation of ECHAM5.

The mass flux coupling preserves flux rates. We associate fluxes from iceberg calving and shelf basal melt with a negative enthalpy flux into the ocean, so that these processes lead to ocean cooling and/or increased sea ice formation.

2.5 Setups and experiments

We performed two fully coupled experiments: LGM-mPISM and PI-mPISM (Tables 1 and 2). LGM-mPISM is the main LGM time slice experiment, PI-mPISM is a pre-industrial control run. With these two experiments we studied the LGM climate, and tested the applicability of the model to two strongly differing climate states.

Coupled ice sheet–climate modeling

F. A. Ziemer et al.

Title Page

Abstract

Introduction

Conclusions

References

Tables

Figures

⏪

⏩

◀

▶

Back

Close

Full Screen / Esc

Printer-friendly Version

Interactive Discussion



In addition, we performed two sensitivity studies: LGM-ICE-5G and LGM-mPISM-W. LGM-ICE-5G is a climate-only experiment with prescribed ICE-5G ice sheet geometry (Peltier, 2004) and follows the PMIP-2 protocol. A comparison of the results with those of LGM-mPISM shows the climatic effects of the interactive ice sheets. In LGM-mPISM-W, we cut the heat fluxes from ice shelf melt and iceberg calving, so the ice enters the ocean as liquid water. The comparison of the model results with LGM-mPISM shows the effects of these heat fluxes for the modeled climate.

In all coupled experiments, the coupling was performed after every year of climate model simulations (10 yr of ISM simulations). The detailed descriptions of the experiments are as follows:

PI-mPISM is an asynchronously coupled experiment under pre-industrial boundary conditions. It serves for the validation of the model and as reference for the LGM simulations. The climate model was started from an existing pre-industrial experiment. The ISM was initialized with the present-day Greenland Ice Sheet shape using PISM's bootstrap methods. The experiment was run for 1000 yr of climate model integration (10 000 yr in the ISM) and the last 100 (1000) yr were analyzed.

LGM-mPISM is an asynchronously coupled experiment under LGM boundary conditions. As spin-up, the ISM was run for several ten-thousand years under prescribed glacial boundary conditions. Then it was coupled with the climate model and run for several thousand years during the different stages of the coupling and tuning process. The last 21 500 ISM-years of this process, the system was fully coupled. The climate model was started from an existing PMIP2-type LGM experiment (Arpe et al., 2011) and run for 3850 yr during the coupling and tuning process (2150 yr fully coupled) before LGM-mPISM was started.

LGM-mPISM-W separates the effect of the latent heat fluxes associated with ice shelf melt and iceberg calving. It is split off from LGM-mPISM after 1650 yr and the latent heat fluxes under investigation are cut, so the ice enters the ocean as liquid water. The experiment has a duration of 700 yr in the climate model (7000 yr in the ISM), the

**Coupled ice
sheet–climate
modeling**

F. A. Ziemer et al.

Title Page

Abstract

Introduction

Conclusions

References

Tables

Figures



Back

Close

Full Screen / Esc

Printer-friendly Version

Interactive Discussion



1899 (pre-industrial) and 1989 to 2010 (ERA INTERIM period) is 0.56 K. The temperature difference over land (-0.8 K) is larger than over the ocean (-0.5 K). The difference also is larger in the high latitudes (-3.2 K north of 45° N, and -1.2 K south of 45° S) than in the low latitudes, where, on the average, the temperature in our model is higher than in the ERA INTERIM reanalysis ($+0.1$ K between 45° S and 45° N).

The smoothed out T31 grid of ECHAM5 is lower than the T255 grid of ERA INTERIM in most mountain areas (the creation of the grid involves spectral smoothing and is not conservative, so the mean surface elevation is lower in a T31 grid than in reality). Differences that can directly be traced back to the lower topography in the T31 resolution of the atmosphere model are the warm biases over the Andes and the Himalaya. Over the Himalaya, typical surface altitude differences between the two model setups are about 500 to 1000 m on the T31 grid, over the Andes, they reach 2000 m, and over the southern tip of Greenland, they reach 1000 m. Assuming a lapse rate of 5 K km^{-1} , as it is used in our coupling scheme, this corresponds to 2.5–5 K temperature difference over the Himalaya, 5–10 K temperature difference over the Andes, and up to 5 K temperature difference over the southern tip of Greenland.

There is a cold bias over the northern Atlantic. This is a consequence of the North Atlantic Current taking a too southerly route. To correctly represent the path of the North Atlantic Current, the ocean model would have to resolve eddies, requiring a horizontal resolution of about 5 km in this region. This is not yet feasible for multi-millennial simulations.

There is a strong cold-bias over the Alaska range, that also occurs in stand-alone simulations (not shown) and becomes stronger because of ice-sheet growth in the coupled setup (Fig. 3). This temperature bias, and thus the glaciation, can be reduced by increasing the climate model resolution (e.g. in the CMIP3-experiments that were performed with a technically identical climate model version), but this is not yet feasible for multi-millennial experiments.

A comparison of the present day annual mean precipitation data from the GPCP dataset (Adler et al., 2003) with PI-mPISM (Fig. 4) shows a good agreement over

Coupled ice sheet–climate modeling

F. A. Ziemer et al.

Title Page

Abstract

Introduction

Conclusions

References

Tables

Figures



Back

Close

Full Screen / Esc

Printer-friendly Version

Interactive Discussion



Greenland. This is also reflected in the agreement of our Greenland mean surface accumulation values with those from regional modeling (Table 3). Over the other polar areas, the values also closely match. The 2-D as well as the zonal mean plots show that most of the precipitation differences occur in the tropics and southern mid-latitudes.

The differences in the tropics are standard modeling artifacts and both regions are not of special interest for this study. In the global mean, the precipitation of 1.03 myr^{-1} is 5% above the GPCP estimate, while north of 45° N the modeled precipitation of 0.66 myr^{-1} is 10% lower than the GPCP estimate.

3.2 The pre-industrial ocean

The North Atlantic Deep Water (NADW) cell of the AMOC (Fig. 5) peaks at 17.0 Sv ($1 \text{ Sv} = 10^6 \text{ m}^3 \text{ s}^{-1}$) at 32.5° N and a depth of 1020 m. This agrees with the estimate of $16 \pm 2 \text{ Sv}$ from Ganachaud (2003) and recent measurements of $18.7 \pm 2 \text{ Sv}$ at 26.5° N (Kanzow et al., 2010). The NADW is formed south of Greenland and in the Greenland-Iceland-Norwegian (GIN) Sea (Fig. 6). The Antarctic Bottom Water (AABW) cell in the Atlantic peaks at 2.9 Sv at 30° S and a depth of 3570 m. The northward heat transport in the Atlantic of 0.86 PW at 23° N is lower than the present day estimates. Ganachaud and Wunsch (2003) obtain $1.27 \pm 0.15 \text{ PW}$ at 24° N as a result of the World Ocean Circulation Experiment (WOCE), and Johns et al. (2011) obtain $1.33 \pm 0.14 \text{ PW}$ at 26° N from the RAPID mooring array measurements. A comparison of the modeled temperatures in the Atlantic and data from WOCE (Koltermann et al., 2011) shows that in our model the deep water flowing southward is warmer than it is in reality. This explains why our model simulates less heat transport than the estimates derived from observations indicate while the overturning strength is similar.

The sea ice maximum and minimum extent agree very well with the long-term average of the HadISST observational data set (Rayner et al., 2003) (Fig. 3).

3.3 The pre-industrial ice sheets

Figure 3 shows the ice sheets in PI-mPISM averaged over the last 1000 yr, as well as the deviations from the reference topography. We obtain a Northern Hemisphere land ice volume of 5.9Mio km^3 , corresponding to 14.9 m of sea level equivalent (SLE) (Table 4). Of this volume, 3.65Mio km^3 (9.2 m SLE) are stored in the Greenland Ice Sheet (see Fig. 12 for the mask used in the analysis). Today's Greenland Ice sheet has a volume of 2.9Mio km^3 (7.3 m SLE). The drift in Greenland Ice sheet volume is $-14\text{ km}^3\text{ yr}^{-1}$. It has a two-dome structure; the main dome reaches a height of 3200 m a.s.l. (above sea level) (3300 m in reality, Bamber et al., 2001) and the southern dome reaches 2700 m a.s.l. (2900 m in reality).

Along most of the coasts of Greenland, the model grows too much ice. At the northern and eastern coast, this is largely due to practically zero ablation from the PDD scheme. The glacier fraction in ECHAM is above 0.5 from the start of the experiment. The grid cells are therefore treated as glaciated, and the surface temperature in these grid cells cannot rise above 0°C . This substantially limits the SAT and thus the melt in the PDD scheme. The sea ice along the northern and eastern coast maintains cold temperatures in the coastal ocean. The temperature is interpolated bilinearly when remapping from ECHAM5 to mPISM. The mean temperature between a sea ice covered grid cell and a glaciated grid cell cannot allow for substantial surface melt. Therefore, the surface mass balance is positive practically all the way to the coast, while substantial ice melt would be needed to stop the glaciers before the coast. There is substantial melt near the western coast where two ECHAM5 grid cells with a glacier fraction below 0.5 remain that are considered as non-glaciated by ECHAM5. An energy balance scheme with detailed treatment of the different heat fluxes (e.g. Vizcaíno et al., 2010) could solve the problems at the east coast, but would have required substantial additional resources. Another way to improve the representation of the Greenland Ice Sheet margins is to use a very fine model resolution ($\ll 5\text{ km}$) in the ISM, that allows resolving the mountain ranges and the individual outlet glaciers.

Coupled ice sheet–climate modeling

F. A. Ziemer et al.

Title Page

Abstract

Introduction

Conclusions

References

Tables

Figures



Back

Close

Full Screen / Esc

Printer-friendly Version

Interactive Discussion



The surface velocities in the northern part of the ice sheet agree reasonably well with the observations of Joughin et al. (2010a, b) (Fig. 7). The ridge of the ice sheet can be seen as a low-velocity band and is very well captured in the northern part. In the central part of the East coast of Greenland, the model shows too much ice because of the lack of ablation described above. This leads to an eastward displacement of the ridge of the ice sheet. Since, at the east coast, the model shows ice in areas that are not glaciated in reality, the flow velocities cannot be compared to observations in this region. In the southeast, there is a massive lack of observations, that prohibits a comparison. In the western part, we capture the general features well, although our velocities generally are too large and the ice sheet reaches further towards the coast than in reality (Fig. 3).

Ice caps form on several Arctic Islands: Baffin Island and Ellesmere Island, Svalbard, Franz Josef Land, Novaya Zemlya, and Severnaya Zemlya. All of these regions presently also show glaciation. There are ice caps with a total volume of 0.94 Mio km^3 ($+86 \text{ km}^3 \text{ yr}^{-1}$) growing in Northeast Siberia and there is an ice sheet with a volume of 1.1 Mio km^3 ($+31 \text{ km}^3 \text{ yr}^{-1}$) in the Alaska Range and the northern Rocky Mountains. In these regions, our climate model shows a cold bias (Fig. 2, Sect. 3.1). This cold bias in regions, that are characterized by many glaciers in reality, leads to a glaciation in mPISM that quickly grows because of the positive feedbacks of increasing altitude and albedo.

3.4 LGM climate experiments

In the following, we discuss the mean state in our LGM model experiments. The results from the asynchronously coupled experiment (LGM-mPISM) are averaged over the full 3 kyr for climate model data, and over the corresponding 30 kyr for ice sheet model data. The mean ice sheet topography in LGM-mPISM is displayed in Fig. 8. To further investigate the climatic effects of the modeled ice sheets, we compare LGM-mPISM with a climate-only experiment with prescribed ice sheets from the ICE-5G reconstruction of Peltier (2004) (Fig. 8, called LGM-ICE-5G in the following), which is consistent

Coupled ice sheet–climate modeling

F. A. Ziemer et al.

Title Page

Abstract

Introduction

Conclusions

References

Tables

Figures



Back

Close

Full Screen / Esc

Printer-friendly Version

Interactive Discussion



with the PMIP-2 protocol. The results from LGM-ICE-5G are averaged over the last 100 yr. For technical details of the setups see Sect. 2.5. The effect of the latent heat flux related to ice shelf melt and iceberg calving is separated in LGM-mPISM-W. The results from LGM-mPISM-W are averaged over the full duration of this experiment and compared with the matching years of LGM-mPISM.

The main differences between the modeled ice sheets in LGM-mPISM and in the ICE-5G reconstruction, that impact the climate are as follows: in ICE-5G as well as in the other reconstructions, the European part of the Fennoscandian Ice Sheet is larger than in LGM-mPISM (Fig. 8), and reaches south across the Baltic and onto the British Isles, while in LGM-mPISM it is limited to Scandinavia and the Barents Sea in the west and reaches far into Northeast Siberia. According to the reconstructions, this region showed only small-scale glaciation. In the course of LGM-mPISM, this extension of the Fennoscandian Ice Sheet connects to an extension of the Laurentide Ice Sheet that has formed over Alaska, the Bering Sea and Kamchatka, closing the gap between the ice sheets. The modeled LIS is thicker in the north and does not reach as far south as in ICE-5G. The ICE-5G reconstruction features a massive North-South-ridge over western Canada that is neither shown by the model, nor by other reconstructions (Sect. 3.7).

The following analysis starts with the atmosphere, then continues with the ocean, and the ice sheets. In addition to the description of the mean state in LGM-mPISM, we provide information about the long-term drift in Sect. 3.8.

3.5 The LGM atmosphere

In LGM-mPISM, the global annual mean SAT is reduced by 3.5K compared with PImPISM (Fig. 2), in agreement with $4.0 \pm 0.8\text{K}$ from a proxy data interpolation by Annan and Hargreaves (2013). As it is typical for the effect of a change in greenhouse gas concentration, the cooling over land (5.4K) is larger than over the oceans (2.5K). If we apply the same T31-land-sea mask to the SAT reconstruction by Annan and Hargreaves

(2013) they obtain 6.3K over land, and 3.0K over ocean areas. Areas that are glaciated in LGM-mPISM cool by 11K, non-glaciated land by 3.3K.

In LGM-mPISM, some regions warm compared to PI-mPISM (Fig. 2). The northern rim of the Pacific, and the northern Atlantic south of 50° N warm in the annual mean. The northern Pacific, warms because of the change in stationary eddies due to topographic changes of the the East Siberian ice sheet. This enhances the advection of warm air from the south. The cloud cover decreases in practically all regions north of 45° N leading to stronger shortwave radiation at the surface. The warming over the Atlantic results from an increase in the oceanic heat transport (Sect. 3.6). Kazakhstan, the Ural Mountains, and the West Siberian Plain warm in summer because of the aforementioned decreased cloud cover that allows more shortwave radiation to reach the ground and overcompensates for the effect of the higher surface albedo and because of less evaporative cooling as a consequence of reduced precipitation.

In LGM-ICE-5G, the cooling is stronger than in LGM-mPISM with a mean of 5.3K compared to PI-mPISM (Fig. 2). This is slightly outside the temperature envelope of $4.0 \pm 0.8K$ provided by Annan and Hargreaves (2013), but within the envelope of the PMIP2 ensemble published in Braconnot et al. (2007). Over the oceans, LGM-ICE-5G cools by 4.1K, over land by 7.7K, over the areas that are glaciated in ICE-5G by 14K, over non-glaciated land by 5.4K.

To understand the temperature differences between LGM-mPISM and LGM-ICE-5G, we split an experiment from LGM-ICE-5G, replaced the topography of LGM-ICE-5G with that of LGM-mPISM, and kept the glacier mask constant at ICE-5G conditions. The SAT increased by 0.87K in years 60 to 90 compared with the same years of LGM-ICE-5G (not shown). This is about half of the 1.6K temperature difference between LGM-ICE-5G and LGM-mPISM. Most of the northern Pacific warms. Over the western part, this is largely a downwind effect of higher temperatures over Asia, while over the eastern part, the picture is less clear with strong regional differences in the partitioning of the heat fluxes (not shown). The higher topography over the Canadian Arctic

Coupled ice sheet–climate modeling

F. A. Ziemer et al.

Title Page

Abstract

Introduction

Conclusions

References

Tables

Figures



Back

Close

Full Screen / Esc

Printer-friendly Version

Interactive Discussion



Archipelago and Greenland cools these regions, and following from that the air over the GIN Sea and the Arctic Ocean.

The global mean precipitation in LGM-mPISM (Fig. 4) of 0.96 myr^{-1} is 7% lower than in PI-mPISM. This difference is especially pronounced in the regions north of 45° N , where the precipitation is reduced by 18% to 0.54 myr^{-1} . The difference in precipitation between LGM-ICE-5G and PI-mPISM is larger (-11% globally, and -31% north of 45° N) because of the lower temperature and the resulting lower atmospheric moisture content.

The 500 hPa geopotential height field in LGM-mPISM (contour lines in Fig. 9b) shows a wavenumber two pattern over the northern extra-tropics with one ridge over western Canada and Alaska, and the second one over the eastern Atlantic reaching into the GIN sea and into Siberia. The troughs are centered over eastern Canada, and Sakhalin Island. The changes compared to PI-mPISM show a wavenumber three pattern (Fig. 9a). They stem from topography and temperature changes. A mountain in a zonal flow creates a high pressure ridge on the upwind side and a trough on the downwind side; lower air temperatures below decrease the geopotential height of a pressure level (Peixoto and Oort, 1992). The Laurentide ice sheet strengthens the dipole pattern over Alaska and Canada. The strong cooling over the GIN Sea and Scandinavia (Fig. 2b) weakens the pressure ridge there, the East Siberian Ice Sheet strengthens the dipole pattern over Siberia. LGM-ICE-5G and LGM-mPISM differ by a wavenumber three pattern (colors in Fig. 9b). The changes largely stem from the different ice sheets (Sect. 3.7). In LGM-mPISM the downwind troughs of the Fennoscandian Ice Sheet and the Siberian Highlands coincide and create a massive trough centered over Sakhalin. Since the Fennoscandian Ice Sheet is restricted to its western part in ICE-5G, the leeward trough falls onto the Siberian high, which shrinks by more than 45 m compared to LGM-mPISM, while the trough over Sakhalin shoals by 70 to 65 m. In contrast to LGM-mPISM, the Laurentide Ice Sheet does not cover Alaska in ICE-5G. Therefore the upwind ridge of the Laurentide Ice Sheet shifts eastward in LGM-ICE-5G. The Laurentide Ice Sheet reaches further to the south in ICE-5G. Its leeward trough also expands

Coupled ice sheet–climate modeling

F. A. Ziemein et al.

Title Page

Abstract

Introduction

Conclusions

References

Tables

Figures



Back

Close

Full Screen / Esc

Printer-friendly Version

Interactive Discussion



**Coupled ice
sheet–climate
modeling**

F. A. Ziemer et al.

[Title Page](#)[Abstract](#)[Introduction](#)[Conclusions](#)[References](#)[Tables](#)[Figures](#)[⏪](#)[⏩](#)[◀](#)[▶](#)[Back](#)[Close](#)[Full Screen / Esc](#)[Printer-friendly Version](#)[Interactive Discussion](#)

southward and weakens the pressure ridge over the Atlantic by more than 45 m. The Laurentide Ice Sheet is lower in the northern parts, therefore the leeward trough over Canada weakens in LGM-ICE-5G. The Scandinavian part of the Fennoscandian ice sheet is higher in the reconstruction than the model and strengthens the upwind pressure ridge over the GIN Sea.

3.6 The LGM ocean

In both LGM experiments, the westward wind stress (Fig. 9) increases over the Irminger Basin (up to +140 mPa compared with PI-mPISM). The eastward wind stress increases over the Labrador Sea. The increase is higher in LGM-ICE-5G (+150 mPa) than in LGM-mPISM (+50 mPa). The wind stress decreases along the coast near Newfoundland (−40 mPa). This decrease is centered slightly further south in LGM-ICE-5G than in LGM-mPISM. Over the Atlantic, the Westerlies slightly shift southward. The southward shift is stronger in LGM-ICE-5G, where the ice sheet reaches further south than in LGM-mPISM. The trade winds over the Atlantic strengthen in both LGM experiments. Over the northern Pacific, the wind stress from the Westerlies strengthens in LGM-mPISM (up to +50 mPa), while it weakens in LGM-ICE-5G (up to −50 mPa). Over the Antarctic Circumpolar Current, the wind stress is higher in LGM-ICE-5G than in LGM-mPISM.

In LGM-mPISM, the NADW is formed southeast of Iceland (Fig. 6b). The NADW cell of the AMOC (Fig. 5b) peaks at 22.1 Sv (PI-mPISM: 17.0 Sv) at 32.5° N in a depth of 1020 m. The NADW cell reaches approximately 65° N. In contrast to PI-mPISM, hardly any deep water is formed in the GIN Sea or in the Labrador Sea. This is indicated by the March mixed layer depth in Fig. 6b. Because of the lack of NADW formation in the GIN Sea, the NADW cell does not extend north of Iceland. The AABW cell strengthens and peaks at 3.6 Sv at 21.5° S and a depth of 3570 m.

In LGM-ICE-5G experiment, the NADW cell (Fig. 5c) is weaker than in LGM-mPISM (Fig. 5a). The streamfunction peaks at 18 Sv at 35.5° N and a depth of 1020 m. The NADW cell is slightly stronger than in PI-mPISM, and, as in LGM-mPISM, it does not

Coupled ice sheet–climate modeling

F. A. Ziemer et al.

[Title Page](#)[Abstract](#)[Introduction](#)[Conclusions](#)[References](#)[Tables](#)[Figures](#)[Back](#)[Close](#)[Full Screen / Esc](#)[Printer-friendly Version](#)[Interactive Discussion](#)

substantially extend beyond Iceland. In contrast to LGM-mPISM, NADW is formed in the Labrador Sea, and in the GIN Sea (Fig. 6), as in PI-mPISM. The deep water formation zone in the GIN Sea is smaller than in PI-mPISM while the deep water formation zone in the Labrador Sea expands. Sensitivity experiments show that it is possible to switch between the LGM-mPISM and the LGM-ICE-5G deep water formation areas by swapping the ice sheets. This indicates that the shape of the ice sheets determines the pattern of deep water formation. Although the maximum of the overturning streamfunction stays at the same depth, the boundary between NADW and AABW shoals slightly. The AABW cell is slightly stronger (3.8 Sv) in LGM-ICE-5G than in LGM-mPISM.

The North Atlantic Subtropical Gyre strengthens in LGM-mPISM compared to PI-mPISM while the Subpolar Gyre weakens (Fig. 10). Increased surface wind stress from the Westerlies shifts the front between the two Gyres northward (Fig. 9c). The barotropic circulation in the GIN Sea is weaker in both LGM experiments (LGM-mPISM and LGM-ICE-5G) than in PI-mPISM. In contrast to LGM-mPISM, in LGM-ICE-5G, the Subpolar Gyre strengthens compared to PI-mPISM (Fig. 10). The difference in Subpolar Gyre strength between LGM-mPISM and LGM-ICE-5G matches with the different deep water formation areas and with the differences in wind stress. While LGM-ICE-5G has substantial deep water formation in the Labrador sea (see above and Fig. 6), that contributes to driving the Subpolar Gyre, in LGM-mPISM the deep water is formed on the north eastern side of the Atlantic. In LGM-ICE-5G, the Antarctic Circumpolar Current strengthens by 25 Sv from 143 to 168 Sv and the AABW formation strengthens.

The ocean heat transport in LGM-mPISM reaches 1.1 PW at 23° N (0.86 PW in PI-mPISM, 1.0 PW in LGM-ICE-5G). Between 15° S and 35° N, the AMOC component dominates the heat transport and the differences between the experiments (Fig. 11). It is highest in LGM-mPISM, where the AMOC is strongest. Outside of this latitude band, the gyre transports become more important. Between 40 and 60° N, the strong Subpolar Gyre dominates the transports in PI-mPISM and LGM-ICE-5G, while in LGM-mPISM, the Subpolar Gyre is weak and the AMOC contributes significantly. All experiments show similar total heat transports in the North Atlantic.

Coupled ice sheet–climate modeling

F. A. Ziemeň et al.

Title Page

Abstract

Introduction

Conclusions

References

Tables

Figures



Back

Close

Full Screen / Esc

Printer-friendly Version

Interactive Discussion



The sea ice in LGM-mPISM reaches further south in the North Atlantic than in PI-mPISM (see Figs. 3 and 8). It reaches Iceland during the entire year and covers large parts of the deep water formation areas of PI-mPISM. The winter sea ice margin reaches 63° N east of Iceland and 43° N at the American east coast. A part of the Labrador Sea becomes ice-free during summer. In LGM-ICE-5G, the winter sea ice is similar to that of LGM-mPISM. The summer sea ice margin shifts to the north, the Norwegian Sea becomes ice-free and the summer sea ice cover in the Labrador Sea decreases (Fig. 8). The reduced summer sea ice cover in LGM-ICE-5G is a combined effect of the missing latent heat flux from glacier melt (see below), and the higher wind stress pushing more ice out of the Labrador Sea (Fig. 9d).

The heat fluxes from glacier calving and shelf basal melt contribute 30% of the total cooling of the Arctic Ocean in LGM-mPISM (Table 5). In LGM-mPISM-W, these heat fluxes are cut. Thus, the ice cover thins (–32% ice thickness) and the ocean loses more heat to the atmosphere (+30%). The total heat loss from the Arctic Ocean sinks by 8%, the ice export through Fram Strait by 16%, the ice volume in the GIN Sea by 24%, and its extent by 8%. The summer sea ice cover in the Labrador Sea shrinks (yellow/orange outline in Fig. 8). These changes explain for a part of the sea ice differences between LGM-ICE-5G and LGM-mPISM.

3.7 The LGM ice sheets

The total modeled land ice volume in the Northern Hemisphere is 60 Mio km³, corresponding to 150 m of sea level change. Table 6 lists the ice sheet volumes, Fig. 12 shows the time evolution of the volumes, and the mask used for this analysis. We compare our results to four reconstructions. The widely used ICE-5G reconstruction (Fig. 8c, Peltier, 2004), its follow-up ICE-6G as provided by the PMIP-3 project (PMIP3 Project members, 2010), the latest reconstruction by Lev Tarasov (Fig. 8b, Tarasov and Peltier, 2003; Tarasov et al., 2012, labeled as Tarasov in the following) and the reconstruction by Kurt Lambeck as provided by the PMIP-3 project (PMIP3 Project members, 2010, ANU in the following). ICE-5G consists of a high-resolution bedrock topography

**Coupled ice
sheet–climate
modeling**

F. A. Ziemeň et al.

[Title Page](#)[Abstract](#)[Introduction](#)[Conclusions](#)[References](#)[Tables](#)[Figures](#)[Back](#)[Close](#)[Full Screen / Esc](#)[Printer-friendly Version](#)[Interactive Discussion](#)

mask we use in mPISM (see Sect. 2.2) does not allow for sliding in the interior of Greenland (blue areas in Fig. 1), the ice streams are limited to the continental shelf. This does not prohibit fast-flowing ice as in PI-mPISM (Fig. 7), where fast ice flow occurs in parts of the Greenland Ice Sheet where the sediment mask prohibits sliding.

5 This fast flow is caused entirely by internal deformation. The inclusion of temperate ice in PISM allows for a very low viscosity, so the ice can reach high speeds by pure internal deformation.

3.7.2 The LGM Laurentide Ice Sheet

10 Baffin Island and Ellesmere Island are fully glaciated in LGM-mPISM and connect the Greenland Ice Sheet to the Laurentide Ice Sheet. The Laurentide Ice Sheet covers present-day Canada and has a mean volume of 31 Mio km^3 (ICE-5G: 36 Mio km^3), corresponding to 78 m of sea level (ICE-5G: 90.7 m SLE). In the west, it terminates inland of the coast, while in the east and north, it fully covers the coasts. The southern boundary is approximately at 50° N in the west and at 45° N in the east. The Laurentide Ice Sheet is split into a main part and a western Cordilleran part by the Mackenzie Ice Stream. This ice stream cuts down to below 1500 m.a.s.l. and is in continuous operation with an average strength of 694 Gt yr^{-1} (21 mSv water equivalent). Over large time fractions, Mackenzie Ice Stream shows net surface melt in its northern part because of a foehn-effect acting on the winds from the Pacific. This area is characterized by very low surface elevations. The main part of the Laurentide Ice Sheet has two domes that are separated by the Hudson Bay. The maximum height of the eastern dome is 3200 m (3600 m of ice thickness), the maximum height of the western dome is 3150 m (also 3600 m of ice thickness). The Hudson Bay area is largely drained by the Hudson Strait Ice Stream that approximately every 7000 yr flushes ice into the Labrador Sea. Unless otherwise noted, we average over this oscillation in this chapter. Details of the oscillation and its implications in the climate system will be covered in a follow-up publication. The main part of the Laurentide Ice Sheet loses ice by surface melt at its southern boundary and by calving into the ocean at the eastern and northern boundaries.

Coupled ice sheet–climate modeling

F. A. Ziemer et al.

Title Page

Abstract

Introduction

Conclusions

References

Tables

Figures



Back

Close

Full Screen / Esc

Printer-friendly Version

Interactive Discussion



The Cordilleran part of the Laurentide Ice Sheet reaches heights of up to 3550 m, but these elevations are reached only on high mountains, so the thickness there is about 1000 m. In valleys, the thickness reaches up to 2700 m, with surface heights of up to 2800 m. The surface accumulation of the Cordilleran part of the Laurentide Ice Sheet is balanced by the Mackenzie Ice Stream on the eastern side and by surface melt on the western side. The melt on the western side is possible because of the high temperature in the northern Pacific, that locally exceed those in PI-mPISM.

None of the reconstructions show an ice-free American west coast. They differ in the southern boundary and in the details of the structure of the interior of the ice sheet. All four reconstructions agree with our model in putting the south-western edge further to the north than the eastern edge, with values for the south-western edge between 42° N (ANU and ICE-6G) and 50° N (Tarasov) (50° N in our model). For the south-eastern edge the values are between 35° N (ANU and ICE-6G) and 40° N (Tarasov and ICE-5G), while our model yields 45° N. Considering that our climate model has a resolution of about 3.75°, this match is acceptable. In the ANU reconstruction and in our model the Mackenzie Ice Stream splits the Laurentide Ice Sheet into a western and an eastern part. In ICE-5G and in the Tarasov reconstruction this ice stream is less well represented. It is hardly discernible in ICE-6G. In the central part, the ANU reconstruction shows a higher surface elevation than our model, but the structure is very similar with a rather low surface elevation in the region of the Hudson Bay and higher surface elevation south and west of it. A similar structure can be seen in the Tarasov reconstruction. West of the Hudson bay, ICE-5G, shows a massive mountain range between 90° W and 120° W, reaching about 4500 m a.s.l. while ICE-6G has a peak in the Hudson Bay area.

A comparison of the ice streams simulated in the model (Fig. 1) with those found in proxy records (Stokes and Tarasov, 2010) shows several ice streams, where models and reconstructions agree. In the following, numbers relate to the numbering in Stokes and Tarasov (2010) and Fig. 1. The central Laurentide Ice Sheet is drained into the Arctic Ocean by Mackenzie Ice Stream (1). There are two major ice streams in the

Canadian Arctic Archipelago, the Amundsen Gulf Ice Stream (18) just to the east of Mackenzie, and M'Clure Strait (19) north of Amundsen Gulf Ice Stream. Both show surge behavior. So does Lancaster Sound Ice Stream (22) with its tributaries, the Admiralty Inlet (21) and the Gulf of Boothia ice stream (20). They drain the north-eastern part of the Laurentide Ice Sheet into Baffin Bay. Further to the south, hardly represented, the Cumberland Sound Ice Stream (23) surges into the Davis Strait. South of Cumberland Sound and well represented, the Hudson Strait Ice Stream (24) drains the Hudson Bay into the Labrador Sea. The Hudson Strait is not the only possible ice stream route for draining the Hudson Bay. The sediment distribution allows for a more northerly route joining the Lancaster Sound Ice Stream and draining into the northern corner of Baffin Bay. However, this route does not become active in our experiments (Fig. 1). A repeatedly surging ice stream drains the Ungava Bay (16) into the Hudson Strait. In the Gulf of St Lawrence, a large ice stream system forms in the Laurentian Channel (25) and neighboring tributaries.

3.7.3 The LGM Eurasian Ice Sheets

The Laurentide Ice Sheet connects via Alaska to an ice sheet in eastern Siberia, that does not exist in the reconstructions. There is however evidence of Pleistocene glaciation of the east Siberian continental margin (Niessen et al., 2013), and of late Pleistocene large-scale glaciation at the Siberian Pacific coast (Bigg et al., 2008; Barr and Clark, 2012). The modeled East Siberian Ice Sheet has a maximum height of 3300 m and a volume of 9.3 Mio km^3 , corresponding to 24 m SLE. The drift is $+108 \text{ km}^3 \text{ yr}^{-1}$. In the model, the East Siberian Ice Sheet closes the gap between the Laurentide Ice Sheet in the East, and the Fennoscandian Ice Sheet in the West. Krinner et al. (2011) concluded that two important factors for not glaciating eastern Siberia are (1) the low snow albedo that is caused by dust deposition, and (2) moisture blocking by the Fennoscandian Ice Sheet. We do not use a locally varying glacier albedo, so the first effect is not represented in our setup. The modeled Fennoscandian Ice Sheet does not reach as far south as indicated by the reconstructions and the coarse resolution of the

CPD

10, 563–624, 2014

Coupled ice sheet–climate modeling

F. A. Ziemeň et al.

Title Page

Abstract

Introduction

Conclusions

References

Tables

Figures



Back

Close

Full Screen / Esc

Printer-friendly Version

Interactive Discussion



Coupled ice sheet–climate modeling

F. A. Ziemer et al.

Title Page

Abstract

Introduction

Conclusions

References

Tables

Figures



Back

Close

Full Screen / Esc

Printer-friendly Version

Interactive Discussion



Atmosphere model does not allow for a realistic simulation of the moisture blocking. Furthermore, we run the model under LGM boundary conditions for a long time span, so our (steady-state) response must be expected to be different from a transient state. The East Siberian Ice Sheet loses mass by surface melt along all margins except for the Arctic Ocean coast, where the losses occur purely by calving and shelf basal melt. Further calving and shelf basal melt occur at the Pacific coast.

The Fennoscandian Ice Sheet has a volume of 11.6 Mio km^3 (29.2 m SLE; ICE-5G: 8.2 Mio km^3 , 20.7 m SLE) and shows a drift of $+156 \text{ km}^3 \text{ yr}^{-1}$. It consists of two main parts. One part covers the Barents, Kara and Laptev Sea shelves and the islands in this region up to Svalbard in the northwestern corner, the other part covers Scandinavia south to 60° N . The eastern part starts with a peak height of 2600 m. During the experiment, the ice sheet expands southward, and the peak shifts to the south and grows to 3000 m. The western part starts with a peak height of 2730 m, decreases to 2600 m during the first 10000 yr and then stabilizes. Along the southern border and parts of the Norwegian Sea coast, there is surface melt. At the Arctic Ocean coast, all losses occur directly into the ocean.

Among the reconstructions of the Fennoscandian Ice Sheet, ICE-5G and ICE-6G show the largest low-thickness zones. Such zones are hard to obtain as a steady state solution in an dynamical ice sheet model, where there are positive feedbacks for ice sheet growth, until either height desertification or a nearby coast limit the ice sheet height. They are easier to obtain as a transient state. The closure of the gap between the Fennoscandian Ice Sheet and the East Siberian Ice Sheet at the end of the coupled experiment shows such a large, flat zone, that is growing by surface accumulation. ICE-5G portrays the Fennoscandian Ice Sheet as reaching far to the south and staying below 1000 m in its southern parts. In the ANU reconstruction, the region between 50 and 60° N is covered with substantially thicker ice exceeding 1500 m in large parts and even exceeding 2500 m over Norway. The surface elevations in the Tarasov reconstruction are lower over Norway and the Barents Sea than in the ANU reconstruction, but the reconstructions largely agree. Over the Barents, Kara, and Laptev Seas, our model

places much more ice than any of the reconstructions. There are massive ice streams between Norway and Svalbard (α) and further streams between the present-day islands at the northern margin of the ice sheet (β, γ). They match with proxy records (Denton and Hughes, 1981). The southern margin ice streams cannot be compared to the reconstructions, since the margin is too far in the north.

Iceland is covered by an ice cap with a volume of $278\,000\text{km}^3$ (0.7 m SLE, ICE-5G: $172\,000\text{km}^3$, resp. 0.43 m SLE) and a maximum height of 2450 m (1400 m ice thickness).

3.8 Long-term changes

In the following, we describe the long-term drift, starting with the ice sheets and then moving on to the atmosphere and finally to the ocean. The recurring surges will be covered in a follow-up publication.

Figure 12 shows the evolution of the ice sheet volumes in LGM-mPISM. The largest changes occur in the Bering Sea Shelf and between the East Siberian and Fennoscandian Ice Sheets. The Bering Sea shelf is flooded with Ice from Alaska between years 9000 and 11000. The ice stream surges transport vast amounts of ice into the region (Fig. 1) and, in the first years, have to compensate for strong surface melt. Over time, the ice sheet stabilizes.

The eastern part of the Fennoscandian Ice Sheet slowly expands southward. This allows the ridge to shift southward and increase in altitude. For the first 20000 ice model years, the snow in the region between the Fennoscandian and the Siberian Ice Sheets melts during the summer, except for a few cold years, when it survives the summer melt. The ice sheets slowly grow into this area by lateral ice advection and start closing the gap from the sides. During the last 10kyr, the winter snow in the gap between the ice sheets survives the summer melt and the gap between the ice sheets is closed by glacier growth from local accumulation.

The closure of the gap between the ice sheets has implications for the atmospheric transports into and out of the Arctic. The SAT north of 70°N decreases with the

CPD

10, 563–624, 2014

Coupled ice sheet–climate modeling

F. A. Ziemer et al.

Title Page

Abstract

Introduction

Conclusions

References

Tables

Figures



Back

Close

Full Screen / Esc

Printer-friendly Version

Interactive Discussion



**Coupled ice
sheet–climate
modeling**

F. A. Ziemer et al.

[Title Page](#)[Abstract](#)[Introduction](#)[Conclusions](#)[References](#)[Tables](#)[Figures](#)[Back](#)[Close](#)[Full Screen / Esc](#)[Printer-friendly Version](#)[Interactive Discussion](#)

strongest changes in the areas of the expansion of the ice sheets. The expansion of the ice sheets strongly increases the local albedo and thereby reduces the absorption of incoming shortwave radiation. At the same time it prevents the outflow of cold air masses towards the Pacific and the inflow of warm air masses from the Pacific. North of 80° N the reduced atmospheric heat input and reduced shortwave absorption lead to a cooling by 0.8 K. The precipitation sinks by 7%. The region south of the ice sheets warms by up to two Kelvin. More shortwave radiation reaches the surface, and the enhanced radiation uptake dominates the warming, while changes in advective heat transports are of minor importance. A similar warming south of ice sheets was found in sensitivity studies by Felzer et al. (1996) and Felzer (2001).

As a second consequence of the gap closure between the Siberian and Laurentide ice sheet, the GIN Sea becomes the only free exit route from the Arctic and the northerly wind over the GIN Sea strengthens. More ice is exported. The additional sea ice reduces the shortwave absorption during summer. The atmospheric heat transport into the GIN sea region increases but cannot compensate for the ice-albedo effect and the whole troposphere cools. The stratification in the Arctic Ocean and the GIN Sea transitions from a three-layer system to a two-layer system. The temperature maximum of the Atlantic inflow is slowly eroded while the deep water warms over time. At the same time, the salinity of the deep water decreases while the salinity at the surface increases. With the weakened stratification, more deep water is formed in the Greenland Sea southwest of Svalbard over time. The atmosphere-ocean heat flux of the Arctic Ocean does not change significantly.

With the growing meridional temperature gradient over the Atlantic, the strength of the NADW cell of the AMOC grows from 20.7 to 23.2 Sv at 30° N during the course of the experiment. Meanwhile the AABW cell shows no long-term drift clearly separable from the variability.

3.9 Comparison to other model coupling studies

Technically, this study extends the work by Vizcaíno et al. (2008, 2010). While these studies focus on the response of the Greenland Ice Sheet to a global warming scenario and the effects of the increased ice melt in the climate system, our focus is on glacial climate dynamics. To represent the physics that is relevant in a glacial setup, we add ice–ocean interaction and use the more advanced ice sheet model mPISM instead of SICOPOLIS. mPISM solves the SIA and the SSA and combines the results. By applying the SSA to ice streams and shelves, mPISM resolves the membrane stresses that are relevant in these areas and thus has a substantially better representation of ice streams and shelves than the SIA-only model SICOPOLIS. We do not model the Antarctic Ice Sheet, but focus on the Northern Hemisphere. In comparison to Vizcaíno et al. (2010), we have to go one step back in the calculation of the surface mass balance and use a PDD model instead of the more advanced energy balance model. The PDD method is much faster and also is widely used in glaciological and coupled model studies (e.g. Gregory et al., 2012).

We are not aware of any published studies where a coupled AOGCM-ISM system is run on a hemispheric scale under LGM maximum boundary conditions. There are studies that come close to this, such as the AOGCM-ISM experiments presented in Gregory et al. (2012), where the AOGCM FAMOUS (a fast version of HadCM3) is coupled with the ice sheet model GLIMMER in a setup that covers the Canadian Arctic Archipelago and Scandinavia to investigate feedbacks in the last glacial inception. Their model is coupled in a way that maximizes glaciation and thus yields substantial glaciation under pre-industrial boundary conditions. Other studies, e.g. Fyke et al. (2011) focus on Greenland and Antarctica. While Siberia does glaciate unrealistically in our model, this process occurs very slowly over several millennia and largely by lateral advection of ice. This could be avoided by taking the effect of dust depositions on temperatures and melt rates into account (Krinner et al., 2011), or by performing a transient simulation.

CPD

10, 563–624, 2014

Coupled ice sheet–climate modeling

F. A. Ziemer et al.

Title Page

Abstract

Introduction

Conclusions

References

Tables

Figures



Back

Close

Full Screen / Esc

Printer-friendly Version

Interactive Discussion



Coupled ice sheet–climate modeling

F. A. Ziemer et al.

[Title Page](#)

[Abstract](#)

[Introduction](#)

[Conclusions](#)

[References](#)

[Tables](#)

[Figures](#)



[Back](#)

[Close](#)

[Full Screen / Esc](#)

[Printer-friendly Version](#)

[Interactive Discussion](#)



Using the EMIC CLIMBER coupled with the ice sheet model SICOPOLIS, Calov et al. (2002) study Heinrich events and Ganopolski and Calov (2011) model full glacial cycles. Since CLIMBER has a very coarse atmosphere resolution, they employ a full energy balance model to compute the surface mass balance and use a moisture balance model to represent the effect of orographic precipitation. While EMICs can be used for long-time simulations at low computational costs, their climate dynamics are highly parametrized and they thus cannot be used for detailed studies of the climate dynamics. This can only be done in coupled AOGCM-ISM experiments.

4 Summary and conclusions

We studied the glacial climate with an interactively coupled AOVGCM–ISM system. Such systems are only beginning to be developed. Therefore, we have modified the state-of-the-art ISM PISM into mPISM, a model that can be used in coupled ice sheet–climate simulations, and coupled it to the AOVGCM ECHAM5/ MPIOM/ LPJ. Both models, as well as the coupling, work without anomaly maps or flux correction. Thus, they can much better represent the nonlinear dynamics of the climate system than models that employ such methods and commonly assume the correction patterns to stay constant under varying climate conditions. In comparison to simulations using earth system models of intermediate complexity EMICs, AOGCMs represent processes of the ocean circulation and atmosphere dynamics in a much more detailed way and with higher spatial and temporal resolution. In contrast to previous AOGCM–ISM simulations (e.g. Gregory et al., 2012), the ISM covers all relevant parts of the Northern Hemisphere. mPISM is a SIA–SSA hybrid model and thus able to model ice streams more realistically than conventional SIA-only ISMs. The ice sheet model is bidirectionally coupled to the atmosphere as well as to the ocean model, enabling the study of the full interactions between the ice sheets and the climate system.

We validated our setup by performing steady-state experiments under pre-industrial boundary conditions (PI-mPISM). The results agree reasonably well with the

Coupled ice sheet–climate modeling

F. A. Ziemer et al.

[Title Page](#)[Abstract](#)[Introduction](#)[Conclusions](#)[References](#)[Tables](#)[Figures](#)[Back](#)[Close](#)[Full Screen / Esc](#)[Printer-friendly Version](#)[Interactive Discussion](#)

observational data. The global mean SAT in PI-mPISM is below that of ERA-INTERIM, representing the lower pre-industrial greenhouse gas concentrations. The NADW cell strength agrees with the estimates obtained from observations. The NADW is formed in the GIN and Labrador Seas. In PI-mPISM, an ice sheet in the Alaska Range forms.

This is due to a resolution dependent cold bias in the atmosphere model in an area characterized by individual glaciers and ice fields.

With the same setup, we performed the first fully coupled multi-millennial steady-state AOVGCM–ISM simulations under LGM boundary conditions (LGM-mPISM). Again, the results agree reasonably well with proxy data. The NADW formation shifts to southeast of Iceland. The heat fluxes from ice shelf basal melt and calving contribute 30% of the cooling of the Arctic Ocean. Cutting them leads to thinning of the sea ice cover and an increase of the ocean–atmosphere heat flux, as well as to a reduction in the summer sea ice cover in the GIN and Labrador Seas. This underlines the importance of representing the latent heat associated with ice losses in climate models.

During the long steady-state LGM simulations, a spurious ice sheet forms in eastern Siberia and Alaska. This is at least partly due to neglecting the albedo effect of dust on snow and ice in our model, which would increase surface ablation in this region and probably prevent ice sheet growth (Warren and Wiscombe, 1980; Krinner et al., 2011). Further advances could be made by using a sophisticated energy balance scheme for the surface mass balance (e.g. Calov et al., 2005; Vizcaíno, 2006) and a higher model resolution that can resolve the small-scale features of the glaciation in these regions. Finally, LGM-mPISM is a multi-millennial integration under constant LGM boundary conditions, while the LGM in reality was a transient state, where the ice sheets and the climate were not in an equilibrium. The ice sheet in Siberia might in part simply be the result of running the model too long under LGM boundary conditions. Modeling the last glacial as a transient process in AOGCMs is a major challenge for the years to come.

When the model is forced with the ICE-5G ice sheet reconstruction, the LGM cooling is stronger than in LGM-mPISM. In contrast to LGM-mPISM, the NADW is largely formed in the Labrador Sea. It is possible to switch between the deep water formation

regions of LGM-mPISM and LGM-ICE-5G by exchanging the ice sheets. This provides a mechanism for obtaining two different ocean circulation states in glacial climate simulations.

The modified Parallel Ice Sheet Model shows strong surge behavior in the Hudson Strait, as well as in several other regions. These surges follow the Heinrich event mechanism described by MacAyeal (1993) and first modeled in 3-D by Calov et al. (2002). The response of the climate system shows the basic features of Heinrich events (Heinrich, 1988; Clement and Peterson, 2008). We currently study the processes relevant for the last deglaciation with the coupled model system.

Acknowledgements. This work was supported by the Max Planck Society for the Advancement of Science and the International Max Planck Research School on Earth System Modelling. Computational resources were made available by the German Climate Computing Center (DKRZ) through support from the German Federal Ministry of Education and Research (BMBF).

Special thanks to Ed Bueller and the PISM group at University of Alaska, Fairbanks, for providing their model and great support for its use.

ERA INTERIM (Dee et al., 2011) climate reanalysis data was provided by the European Centre for midrange weather forecasts (ECMWF).

Precipitation data from the GPCP project was obtained through the integrated climate data center of the KlimaCampus Hamburg. The GPCP combined precipitation data were developed and computed by the NASA/Goddard Space Flight Center's Laboratory for Atmospheres as a contribution to the GEWEX Global Precipitation Climatology Project.

The service charges for this open access publication have been covered by the Max Planck Society.

CPD

10, 563–624, 2014

Coupled ice sheet–climate modeling

F. A. Ziemer et al.

Title Page

Abstract

Introduction

Conclusions

References

Tables

Figures



Back

Close

Full Screen / Esc

Printer-friendly Version

Interactive Discussion



References

- Abe-Ouchi, A., Segawa, T., and Saito, F.: Climatic Conditions for modelling the Northern Hemisphere ice sheets throughout the ice age cycle, *Clim. Past*, 3, 423–438, doi:10.5194/cp-3-423-2007, 2007. 565, 566, 571
- 5 Abe-Ouchi, A., Saito, F., Kawamura, K., Raymo, M. E., Okuno, J., Takahashi, K., and Blatter, H.: Insolation-driven 100,000-year glacial cycles and hysteresis of ice-sheet volume, *Nature*, 500, 190–193, doi:10.1038/nature12374, 2013. 566
- Adler, R. F., Huffman, G. J., Chang, A., Ferraro, R., Xie, P.-P., Janowiak, J., Rudolf, B., Schneider, U., Curtis, S., Bolvin, D., Gruber, A., Susskind, J., Arkin, P., and
10 Nelkin, E.: The Version-2 Global Precipitation Climatology Project (GPCP) monthly precipitation analysis (1979–present), *J. Hydrometeorol.*, 4, 1147–1167, doi:10.1175/1525-7541(2003)004<1147:TVGPCP>2.0.CO;2, 2003. 576, 616
- Amante, C. and Eakins, B. W.: ETOPO1 1 Arc-Minute Global Relief Model: Procedures, Data Sources and Analysis, Tech. rep., NOAA Technical Memorandum NESDIS NGDC-24, National Geophysical Data Center Marine Geology and Geophysics Division, Boulder, Colorado, 2009. 615, 619
- 15 Annan, J. D. and Hargreaves, J. C.: A new global reconstruction of temperature changes at the Last Glacial Maximum, *Clim. Past*, 9, 367–376, doi:10.5194/cp-9-367-2013, 2013. 580, 581
- Arpe, K., Leroy, S. A. G., and Mikolajewicz, U.: A comparison of climate simulations for the
20 last glacial maximum with three different versions of the ECHAM model and implications for summer-green tree refugia, *Clim. Past*, 7, 91–114, doi:10.5194/cp-7-91-2011, 2011. 574
- Aschwanden, A., Bueler, E., Khroulev, C., and Blatter, H.: An enthalpy formulation for glaciers and ice sheets, *J. Glaciol.*, 58, 441–457, doi:10.3189/2012JoG11J088, 2012. 569
- Bamber, J. L., Layberry, R. L., and Gogineni, S. P.: A new ice thickness and bed data set for the Greenland ice sheet 1. Measurement, data reduction, and errors, *J. Geophys. Res.*, 106, 33773–33780, doi:10.1029/2001JD900054, 2001. 578, 610
- 25 Barr, I. D. and Clark, C. D.: Late quaternary glaciations in Far NE Russia; combining moraines, topography and chronology to assess regional and global glaciation synchrony, *Quaternary Sci. Rev.*, 53, 72–87, doi:10.1016/j.quascirev.2012.08.004, 2012. 589
- 30 Bigg, G. R., Clark, C. D., and Hughes, A. L. C.: A last glacial ice sheet on the Pacific Russian coast and catastrophic change arising from coupled ice–volcanic interaction, *Earth Planet. Sc. Lett.*, 265, 559–570, doi:10.1016/j.epsl.2007.10.052, 2008. 589

**Coupled ice
sheet–climate
modeling**

F. A. Ziemeň et al.

[Title Page](#)[Abstract](#)[Introduction](#)[Conclusions](#)[References](#)[Tables](#)[Figures](#)[⏪](#)[⏩](#)[◀](#)[▶](#)[Back](#)[Close](#)[Full Screen / Esc](#)[Printer-friendly Version](#)[Interactive Discussion](#)

Bonelli, S., Charbit, S., Kageyama, M., Woillez, M.-N., Ramstein, G., Dumas, C., and Quiquet, A.: Investigating the evolution of major Northern Hemisphere ice sheets during the last glacial-interglacial cycle, *Clim. Past*, 5, 329–345, doi:10.5194/cp-5-329-2009, 2009. 567

Box, J. E., Bromwich, D. H., Veenhuis, B. A., Bai, L.-S., Stroeve, J. C., Rogers, J. C., Steffen, K., Haran, T., and Wang, S.-H.: Greenland Ice Sheet surface mass balance variability (1988–2004) from calibrated polar MM5 output, *J. Climate*, 19, 2783–2800, doi:10.1175/JCLI3738.1, 2006. 609

Braconnot, P., Otto-Bliesner, B., Harrison, S., Joussaume, S., Peterchmitt, J.-Y., Abe-Ouchi, A., Crucifix, M., Driesschaert, E., Fichet, Th., Hewitt, C. D., Kageyama, M., Kitoh, A., Laîné, A., Loutre, M.-F., Marti, O., Merkel, U., Ramstein, G., Valdes, P., Weber, S. L., Yu, Y., and Zhao, Y.: Results of PMIP2 coupled simulations of the Mid-Holocene and Last Glacial Maximum – Part 1: experiments and large-scale features, *Clim. Past*, 3, 261–277, doi:10.5194/cp-3-261-2007, 2007. 565, 581

Braconnot, P., Harrison, S. P., Otto-Bliesner, B. L., Abe-Ouchi, A., Jungclaus, J. H., and Peterchmitt, J.-Y.: The Paleoclimate Modeling Intercomparison Project contribution to CMIP5, CLIVAR Exchanges, International CLIVAR Project Office National Oceanography Centre European Way, Southampton, UK, 15–19., 2011. 565

Braconnot, P., Harrison, S. P., Kageyama, M., Bartlein, P. J., Masson-Delmotte, V., Abe-Ouchi, A., Otto-Bliesner, B., and Zhao, Y.: Evaluation of climate models using palaeoclimatic data, *Nat. Clim. Change*, 2, 417–424, doi:10.1038/nclimate1456, 2012. 565

Braithwaite, R. J. and Olesen, O. B.: *Glacier Fluctuations and Climatic Change*, in: *Glacier Fluctuations and Climatic Change*, Kluwer, Dordrecht, the Netherlands, 219–233, 1989. 571

Budd, W. F. and Smith, I. N.: The growth and retreat of ice sheets in response to orbital radiation changes, in: *Proceedings of the Canberra Symposium*, December 1979, no. 131 in IAHS Publ., Canberra, 369–409, 1979. 571

Bueler, E. and Brown, J.: Shallow shelf approximation as a sliding law in a thermomechanically coupled ice sheet model, *J. Geophys. Res.*, 114, F03008, doi:10.1029/2008JF001179, 2009. 569

Calov, R.: *Das thermomechanische Verhalten des groenlaendischen Eisschildes unter der Wirkung verschiedener Klimaszenarien – Antworten eines theoretisch-numerischen Modells*, Ph.D. thesis, Institut fuer Mechanik, Technische Hochschule Darmstadt, Darmstadt, Germany, 1994. 571

Coupled ice sheet–climate modeling

F. A. Ziemeň et al.

Title Page

Abstract

Introduction

Conclusions

References

Tables

Figures



Back

Close

Full Screen / Esc

Printer-friendly Version

Interactive Discussion

- Calov, R. and Greve, R.: A semi-analytical solution for the positive degree-day model with stochastic temperature variations, *J. Glaciol.*, 51, 173–175, 2005. 572
- Calov, R., Ganopolski, A., Petoukhov, V., Claussen, M., and Greve, R.: Large-scale instabilities of the Laurentide ice sheet simulated in a fully coupled climate-system model, *Geophys. Res. Lett.*, 29, 69-1–69-4, doi:10.1029/2002GL016078, 2002. 567, 570, 594, 596
- Calov, R., Ganopolski, A., Claussen, M., Petoukhov, V., and Greve, R.: Transient simulation of the last glacial inception – Part I: Glacial inception as a bifurcation in the climate system, *Clim. Dynam.*, 24, 545–561, doi:10.1007/s00382-005-0007-6, 2005. 567, 595
- Charbit, S., Ritz, C., Philippon, G., Peyaud, V., and Kageyama, M.: Numerical reconstructions of the Northern Hemisphere ice sheets through the last glacial-interglacial cycle, *Clim. Past*, 3, 15–37, doi:10.5194/cp-3-15-2007, 2007. 566
- Clark, P. U., Dyke, A. S., Shakun, J. D., Carlson, A. E., Clark, J., Wohlfarth, B., Mitrovica, J. X., Hostetler, S. W., and McCabe, A. M.: The Last Glacial Maximum, *Science*, 325, 710–714, doi:10.1126/science.1172873, 2009. 565
- Clement, A. C. and Peterson, L. C.: Mechanisms of abrupt climate change of the last glacial period, *Rev. Geophys.*, 46, RG4002, doi:10.1029/2006RG000204, 2008. 596
- Dee, D. P., Uppala, S. M., Simmons, A. J., Berrisford, P., Poli, P., Kobayashi, S., Andrae, U., Balmaseda, M. A., Balsamo, G., Bauer, P., Bechtold, P., Beljaars, A. C. M., van de Berg, L., Bidlot, J., Bormann, N., Delsol, C., Dragani, R., Fuentes, M., Geer, A. J., Haimberger, L., Healy, S. B., Hersbach, H., Hólm, E. V., Isaksen, L., Kållberg, P., Köhler, M., Matricardi, M., McNally, A. P., Monge-Sanz, B. M., Morcrette, J.-J., Park, B.-K., Peubey, C., de Rosnay, P., Tavolato, C., Thépaut, J.-N., and Vitart, F.: The ERA-Interim reanalysis: configuration and performance of the data assimilation system, *Q. J. Roy. Meteorol. Soc.*, 137, 553–597, doi:10.1002/qj.828, 2011. 575, 596
- Denton, G. H. and Hughes, T. J.: *The Last Great Ice Sheets*, edited by: Denton, G. H. and Hughes, T. J., John Wiley, New York, 1981. 591
- Ettema, J., van den Broeke, M. R., van Meijgaard, E., van de Berg, W. J., Bamber, J. L., Box, J. E., and Bales, R. C.: Higher surface mass balance of the Greenland ice sheet revealed by high-resolution climate modeling, *Geophys. Res. Lett.*, 36, L12501, doi:10.1029/2009GL038110, 2009. 609
- Fausto, R. S., Ahlstrøm, A. P., van As, D., and Steffen, K.: Present-day temperature standard deviation parameterization for Greenland, *J. Glaciol.*, 57, 1181–1183, 2011. 571

Coupled ice sheet–climate modeling

F. A. Ziemer et al.

Title Page

Abstract

Introduction

Conclusions

References

Tables

Figures



Back

Close

Full Screen / Esc

Printer-friendly Version

Interactive Discussion

- Felzer, B.: Climate impacts of an ice sheet in East Siberia during the Last Glacial Maximum, *Quaternary Sci. Rev.*, 20, 437–447, doi:10.1016/S0277-3791(00)00106-2, 2001. 592
- Felzer, B., Oglesby, R. J., Webb, T., and Hyman, D. E.: Sensitivity of a general circulation model to changes in Northern Hemisphere ice sheets, *J. Geophys. Res.-Atmos.*, 101, 19077–19092, doi:10.1029/96JD01219, 1996. 592
- Fettweis, X.: Reconstruction of the 1979–2006 Greenland ice sheet surface mass balance using the regional climate model MAR, *The Cryosphere*, 1, 21–40, doi:10.5194/tc-1-21-2007, 2007. 609
- Fichefet, T., Poncin, C., Goosse, H., Huybrechts, P., Janssens, I., and Le Treut, H.: Implications of changes in freshwater flux from the Greenland ice sheet for the climate of the 21st century, *Geophys. Res. Lett.*, 30, 1911, doi:10.1029/2003GL017826, 2003. 567
- Fyke, J. G., Weaver, A. J., Pollard, D., Eby, M., Carter, L., and Mackintosh, A.: A new coupled ice sheet/climate model: description and sensitivity to model physics under Eemian, Last Glacial Maximum, late Holocene and modern climate conditions, *Geosci. Model Dev.*, 4, 117–136, doi:10.5194/gmd-4-117-2011, 2011. 593
- Ganachaud, A.: Large-scale mass transports, water mass formation, and diffusivities estimated from World Ocean Circulation Experiment (WOCE) hydrographic data, *J. Geophys. Res.*, 108, 3213, doi:10.1029/2002JC001565, 2003. 577
- Ganachaud, A. and Wunsch, C.: Large-scale ocean heat and freshwater transports during the world ocean circulation experiment, *J. Climate*, 16, 696–705, doi:10.1175/1520-0442(2003)016<0696:LSOHAF>2.0.CO;2, 2003. 577
- Ganopolski, A. and Calov, R.: The role of orbital forcing, carbon dioxide and regolith in 100 kyr glacial cycles, *Clim. Past*, 7, 1415–1425, doi:10.5194/cp-7-1415-2011, 2011. 567, 594
- Ganopolski, A., Calov, R., and Claussen, M.: Simulation of the last glacial cycle with a coupled climate ice-sheet model of intermediate complexity, *Clim. Past*, 6, 229–244, doi:10.5194/cp-6-229-2010, 2010. 567
- Gregory, J. M., Browne, O. J. H., Payne, A. J., Ridley, J. K., and Rutt, I. C.: Modelling large-scale ice-sheet–climate interactions following glacial inception, *Clim. Past*, 8, 1565–1580, doi:10.5194/cp-8-1565-2012, 2012. 567, 593, 594
- Greve, R.: Application of a polythermal three-dimensional ice sheet model to the Greenland Ice Sheet: response to steady-state and transient climate scenarios, *J. Climate*, 10, 901–918, doi:10.1175/1520-0442(1997)010<0901:AOAPTD>2.0.CO;2, 1997. 566

Coupled ice sheet–climate modeling

F. A. Ziemer et al.

Title Page

Abstract

Introduction

Conclusions

References

Tables

Figures



Back

Close

Full Screen / Esc

Printer-friendly Version

Interactive Discussion

- Hagemann, S. and Dümenil, L.: A parametrization of the lateral waterflow for the global scale, *Clim. Dynam.*, 14, 17–31, doi:10.1007/s003820050205, 1998. 569
- Hagemann, S. and Gates, L. D.: Improving a subgrid runoff parameterization scheme for climate models by the use of high resolution data derived from satellite observations, *Clim. Dynam.*, 21, 349–359, doi:10.1007/s00382-003-0349-x, 2003. 569
- Heinrich, H.: Origin and consequences of cyclic ice rafting in the Northeast Atlantic Ocean during the past 130,000 years, *Quaternary Res.*, 29, 142–152, doi:10.1016/0033-5894(88)90057-9, 1988. 596
- Holland, D. M. and Jenkins, A.: Modeling thermodynamic ice–ocean interactions at the base of an ice shelf, *J. Phys. Oceanogr.*, 29, 1787–1800, doi:10.1175/1520-0485(1999)029<1787:MTIOIA>2.0.CO;2, 1999. 572
- Huybrechts, P., Janssens, I., Poncin, C., and Fichet, T.: The response of the Greenland ice sheet to climate changes in the 21st century by interactive coupling of an AOGCM with a thermomechanical ice-sheet model, *Ann. Glaciol.*, 35, 409–415, 2002. 567
- Johns, W. E., Baringer, M. O., Beal, L. M., Cunningham, S. A., Kanzow, T., Bryden, H. L., Hirschi, J. J. M., Marotzke, J., Meinen, C. S., Shaw, B., and Curry, R.: Continuous, array-based estimates of Atlantic Ocean heat transport at 26.5° N, *J. Climate*, 24, 2429–2449, doi:10.1175/2010JCLI3997.1, 2011. 577
- Joughin, I., Smith, B., and Howat, I.: MEaSURES Greenland Ice Sheet Velocity Map from InSAR Data, available at: <http://nsidc.org/> (last access: 5 February 2014), 2010a. 579
- Joughin, I., Smith, B., Howat, I., and Scambos, T.: MEaSURES Greenland Ice Velocity Map from InSAR Data, NASA DAAC at the National Snow and Ice Data Center, Boulder, Colorado, USA, doi:10.5067/MEASURES/CRYOSPHERE/nsidc-0478.001, 2010b. 579, 619
- Jungclaus, J. H., Keenlyside, N., Botzet, M., Haak, H., Luo, J.-J., Latif, M., Marotzke, J., Mikolajewicz, U., and Roeckner, E.: Ocean circulation and tropical variability in the coupled model ECHAM5/MPI-OM, *J. Climate*, 19, 3952–3972, doi:10.1175/JCLI3827.1, 2006. 569
- Kanzow, T., Cunningham, S. A., Johns, W. E., Hirschi, J. J. M., Marotzke, J., Baringer, M. O., Meinen, C. S., Chidichimo, M. P., Atkinson, C., Beal, L. M., Bryden, H. L., and Collins, J.: Seasonal variability of the Atlantic meridional overturning circulation at 26.5 degrees N, *J. Climate*, 23, 5678–5698, doi:10.1175/2010JCLI3389.1, 2010. 577
- Kim, S. J.: The effect of atmospheric CO₂ and ice sheet topography on LGM climate, *Clim. Dynam.*, 22, 639–651, doi:10.1007/s00382-004-0412-2, 2004. 565

Coupled ice sheet–climate modeling

F. A. Ziemer et al.

Title Page

Abstract

Introduction

Conclusions

References

Tables

Figures

◀

▶

◀

▶

Back

Close

Full Screen / Esc

Printer-friendly Version

Interactive Discussion



Kim, S.-J., Crowley, T., Erickson, D., Govindasamy, B., Duffy, P., and Lee, B.: High-resolution climate simulation of the last glacial maximum, *Clim. Dynam.*, 31, 1–16, doi:10.1007/s00382-007-0332-z, 2008. 614

5 Koltermann, K. P., Gouretski, V. V., and Jancke, K.: Hydrographic Atlas of the World Ocean Circulation Experiment (WOCE), Volume 3: Atlantic Ocean, International WOCE Project Office, Southampton, UK, 2011. 577

Krinner, G., Diekmann, B., Colleoni, F., and Stauch, G.: Global, regional and local scale factors determining glaciation extent in Eastern Siberia over the last 140,000 years, *Quaternary Sci. Rev.*, 30, 821–831, doi:10.1016/j.quascirev.2011.01.001, 2011. 589, 593, 595

10 Laske, G. and Masters, G.: A Global Digital Map of Sediment Thickness, *EOS Trans. AGU*, 78, F483, 1997. 570, 613

Le Meur, E., and Huybrechts, P.: A comparison of different ways of dealing with isostasy: examples from modelling the Antarctic ice sheet during the last glacial cycle, *Ann. Glaciol.*, 23, 309–317, 1996. 570

15 Lemke, P., Ren, J., Alley, R. B., Allison, I., Carrasco, J., Flato, G., Fujii, Y., Kaser, G., Mote, P., Thomas, R., and Zhang, T.: Observations: changes in snow, ice and frozen ground, in: *Climate Change 2007: The Physical Science Basis*, Contribution of the Working Group I to the Fourth Assessment Report of the Intergovernmental Panel on Climate Change, Cambridge University Press, Cambridge, UK, New York, NY, USA, 2007. 610

20 MacAyeal, D. R.: Binge/Purge oscillations of the Laurentide Ice Sheet as a cause of the North Atlantic's Heinrich Events, *Paleoceanography*, 8, 775–784, doi:10.1029/93PA02200, 1993. 596

Marsiat, I.: Simulation of the Northern Hemisphere continental ice sheets over the last glacial-interglacial cycle: experiments with a latitude-longitude vertically integrated ice sheet model coupled to a zonally averaged climate model, *Paleoclim. Data Model.*, 1, 59–98, 1994. 571

25 Marsland, S. J., Haak, H., Jungclaus, J. H., Latif, M., and Röske, F.: The Max-Planck-Institute global ocean/sea ice model with orthogonal curvilinear coordinates, *Ocean Model.*, 5, 91–127, doi:10.1016/S1463-5003(02)00015-X, 2003. 569

30 Mikolajewicz, U., Gröger, M., Maier-Reimer, E., Schurgers, G., Vizcaíno, M., and Winguth, A.: Long-term effects of anthropogenic CO₂ emissions simulated with a complex earth system model, *Clim. Dynam.*, 28, 599–633, doi:10.1007/s00382-006-0204-y, 2007a. 567, 569

Coupled ice sheet–climate modeling

F. A. Ziemeň et al.

Title Page

Abstract

Introduction

Conclusions

References

Tables

Figures

◀

▶

◀

▶

Back

Close

Full Screen / Esc

Printer-friendly Version

Interactive Discussion

- Mikolajewicz, U., Vizcaíno, M., Jungclauss, J., and Schurgers, G.: Effect of ice sheet interactions in anthropogenic climate change simulations, *Geophys. Res. Lett.*, 34, L18706, doi:10.1029/2007GL031173, 2007b. 567, 568
- Niessen, F., Hong, J. K., Hegewald, A., Matthiessen, J., Stein, R., Kim, H., Kim, S., Jensen, L., Jokat, W., Nam, S.-I., and Kang, S.-H.: Repeated Pleistocene glaciation of the East Siberian continental margin, *Nat. Geosci.*, 6, 842–846, doi:10.1038/ngeo1904, 2013. 589
- Pausata, F. S. R., Li, C., Wettstein, J. J., Kageyama, M., and Nisancioglu, K. H.: The key role of topography in altering North Atlantic atmospheric circulation during the last glacial period, *Clim. Past*, 7, 1089–1101, doi:10.5194/cp-7-1089-2011, 2011. 565
- Peixoto, J. P. and Oort, A. H.: *Physics of Climate*, American Institute of Physics, edited by: Peixoto, J. P. and Oort, A. H., Am. Inst. of Phys., New York, 1992. 582
- Peltier, W. R.: Global glacial isostasy and the surface of the ice-age earth: the ice-5G (VM2) model and grace, *Annu. Rev. Earth Pl. Sc.*, 32, 111–149, doi:10.1146/annurev.earth.32.082503.144359, 2004. 570, 574, 579, 585, 586, 612, 620
- PMIP3 Project members: Ice Sheet for PMIP3/CMIP5 simulations, available at: <https://wiki.lscce.ipsl.fr/pmip3/doku.php/pmip3:design:pi:final:icesheet> (last access: 5 February 2014), 2010. 585
- Pollard, D.: A simple ice sheet model yields realistic 100 kyr glacial cycles, *Nature*, 296, 334–338, doi:10.1038/296334a0, 1982. 566
- Pollard, D.: A retrospective look at coupled ice sheet–climate modeling, *Climatic Change*, 100, 173–194, doi:10.1007/s10584-010-9830-9, 2010. 566
- Pollard, D. and DeConto, R. M.: Modelling West Antarctic ice sheet growth and collapse through the past five million years, *Nature*, 458, 329–332, doi:10.1038/nature07809, 2009. 566
- Pollard, D., Muszynski, I., Schneider, S. H., and Thompson, S. L.: Asynchronous coupling of ice-sheet and atmospheric forcing models, *Ann. Glaciol.*, 14, 247–251, 1990. 567
- Rayner, N. A., Parker, D. E., Horton, E. B., Folland, C. K., Alexander, L. V., Rowell, D. P., Kent, E. C., and Kaplan, A.: Global analyses of sea surface temperature, sea ice, and night marine air temperature since the late nineteenth century, *J. Geophys. Res.*, 108, 4407, doi:10.1029/2002JD002670, 2003. 577, 615
- Reeh, N.: Parameterization of melt rate and surface temperature on the Greenland Ice Sheet, *Polarforschung*, 59, 113–128, 1991. 572

Coupled ice sheet–climate modeling

F. A. Ziemeň et al.

Title Page

Abstract

Introduction

Conclusions

References

Tables

Figures

◀

▶

◀

▶

Back

Close

Full Screen / Esc

Printer-friendly Version

Interactive Discussion



- Ridley, J. K., Huybrechts, P., Gregory, J. M., and Lowe, J. A.: Elimination of the Greenland Ice Sheet in a high CO₂ climate, *J. Climate*, 18, 3409–3427, doi:10.1175/JCLI3482.1, 2005. 567
- Rind, D.: Components of the ice age circulation, *J. Geophys. Res.-Atmos.*, 92, 4241–4281, doi:10.1029/JD092iD04p04241, 1987. 565
- 5 Roberts, D. H., Long, A. J., Schnabel, C., Davies, B. J., Xu, S., Simpson, M. J. R., and Huybrechts, P.: Ice sheet extent and early deglacial history of the south-western sector of the Greenland Ice Sheet, *Quaternary Sci. Rev.*, 28, 2760–2773, doi:10.1016/j.quascirev.2009.07.002, 2009. 586
- Roeckner, E., Bäuml, G., Bonventura, L., Brokov, R., Esch, M., Giorgetta, M., Hagemann, S., 10 Kirchner, I., Kornblüeh, L., Manzini, E., Rhodin, A., Schlese, U., Schulzweida, U., and Tompkins, A.: The atmospheric general circulation model ECHAM5 Part 1 Model description, Tech. Rep. 349, Max-Planck-Institut für Meteorologie, Hamburg, 2003. 568
- Schmittner, A., Urban, N. M., Shakun, J. D., Mahowald, N. M., Clark, P. U., Bartlein, P. J., 15 Mix, A. C., and Rosell-Melé, A.: Climate sensitivity estimated from temperature reconstructions of the Last Glacial Maximum, *Science*, 334, 1385–1388, doi:10.1126/science.1203513, 2011. 614
- Schurgers, G., Mikolajewicz, U., Groeger, M., Maier-Reimer, E., Vizcaino, M., and Winguth, A.: The effect of land surface changes on Eemian climate, *Clim. Dynam.*, 29, 357–373, doi:10.1007/s00382-007-0237-x, 2007. 569
- 20 Sitch, S., Smith, B., Prentice, I. C., Arneeth, A., Bondeau, A., Cramer, W., Kaplan, J. O., Levis, S., Lucht, W., Sykes, M. T., Thonicke, K., and Venevsky, S.: Evaluation of ecosystem dynamics, plant geography and terrestrial carbon cycling in the LPJ dynamic global vegetation model, *Global Change Biol.*, 9, 161–185, doi:10.1046/j.1365-2486.2003.00569.x, 2003. 569
- Stokes, C. R. and Tarasov, L.: Ice streaming in the Laurentide Ice Sheet: a first comparison 25 between data-calibrated numerical model output and geological evidence, *Geophys. Res. Lett.*, 37, L01501, doi:10.1029/2009GL040990, 2010. 588, 613
- Tarasov, L. and Peltier, W. R.: Terminating the 100 kyr ice age cycle, *J. Geophys. Res.*, 102, 21665–21693, doi:10.1029/97JD01766, 1997. 566
- Tarasov, L. and Peltier, W. R.: Greenland glacial history, borehole constraints and Eemian extent, *J. Geophys. Res.*, 108, 2124–2143, 2003. 585
- 30 Tarasov, L., Dyke, A. S., Neal, R. M., and Peltier, W. R.: A data-calibrated distribution of deglacial chronologies for the North American ice complex from glaciological modeling, *Earth Planet. Sc. Lett.*, 315–316, 30–40, doi:10.1016/j.epsl.2011.09.010, 2012. 566, 585

Coupled ice sheet–climate modeling

F. A. Ziemer et al.

Title Page

Abstract

Introduction

Conclusions

References

Tables

Figures

◀

▶

◀

▶

Back

Close

Full Screen / Esc

Printer-friendly Version

Interactive Discussion



- the PISM authors: PISM, a Parallel Ice Sheet Model, available at: <http://www.pism-docs.org> (last access: 5 February 2014), 2013. 569
- Valcke, S., Caubel, A., Vogelsang, R., and Declat, D.: OASIS3 User's Guide 5th Edition, Tech. Rep. TR/CMGC/03/69, CERFACS, available at: <http://www.pism.enes.org/Publications/Reports/Report02.pdf> (last access: 5 February 2014), 2004. 569
- Valdes, P.: Built for stability, *Nat. Geosci.*, 4, 414–416, doi:10.1038/ngeo1200, 2011. 565
- Vizcaíno, M.: Long-term interactions between ice sheets and climate under anthropogenic greenhouse forcing – Simulations with two complex Earth System Models, Ph.D. thesis, Universität Hamburg/Max Planck Institut für Meteorologie, available at: http://www.earthsystemschool.mpg.de/fileadmin/user_upload/Documents/Theses/Thesis_Vizcaino.pdf (last access: 5 February 2014), 2006. 595
- Vizcaíno, M., Mikolajewicz, U., Gröger, M., Maier-Reimer, E., Schurgers, G., and Winguth, A.: Long-term ice sheet–climate interactions under anthropogenic greenhouse forcing simulated with a complex Earth System Model, *Clim. Dynam.*, 31, 665–690, doi:10.1007/s00382-008-0369-7, 2008. 567, 593
- Vizcaíno, M., Mikolajewicz, U., Jungclaus, J., and Schurgers, G.: Climate modification by future ice sheet changes and consequences for ice sheet mass balance, *Clim. Dynam.*, 34, 301–324, doi:10.1007/s00382-009-0591-y, 2010. 567, 568, 578, 593
- Wang, Z. and Mysak, L. A.: Simulation of the last glacial inception and rapid ice sheet growth in the McGill Paleoclimate Model, *Geophys. Res. Lett.*, 29, 2102, doi:10.1029/2002GL015120, 2002. 567
- Warren, S. G. and Wiscombe, W. J.: A model for the spectral albedo of snow, II: Snow containing atmospheric aerosols, *J. Atmos. Sci.*, 37, 2734–2745, doi:10.1175/1520-0469(1980)037<2734:AMFTSA>2.0.CO;2, 1980. 595
- Wilken, M. and Mienert, J.: Submarine glacial debris flows, deep-sea channels and past ice-stream behaviour of the East Greenland continental margin, *Quaternary Sci. Rev.*, 25, 784–810, doi:10.1016/j.quascirev.2005.06.004, 2006. 586
- Winkelmann, R., Martin, M. A., Haseloff, M., Albrecht, T., Bueler, E., Khroulev, C., and Levermann, A.: The Potsdam Parallel Ice Sheet Model (PISM-PIK) – Part 1: Model description, *The Cryosphere*, 5, 715–726, doi:10.5194/tc-5-715-2011, 2011. 570

Ziemen, F. A.: Glacial Climate Dynamics, Ph.D. thesis, Universität Hamburg, International Max Planck Research School on Earth System Sciences, available at: http://www.mpimet.mpg.de/fileadmin/publikationen/Reports/WEB_BzE_139.pdf (last access: 5 February 2014), 2013. 569

- 5 Zweck, C. and Huybrechts, P.: Modeling the marine extent of Northern Hemisphere ice sheets during the last glacial cycle, *Ann. Glaciol.*, 37, 173–180, doi:10.3189/172756403781815870, 2003. 566

CPD

10, 563–624, 2014

Coupled ice sheet–climate modeling

F. A. Ziemen et al.

Title Page

Abstract

Introduction

Conclusions

References

Tables

Figures



Back

Close

Full Screen / Esc

Printer-friendly Version

Interactive Discussion



Coupled ice sheet–climate modeling

F. A. Ziemer et al.

Table 1. Main experiments performed and analyzed. For the boundary conditions see Table 2. 1 : 10 coupling means 1 climate model (CM) year per 10 ice sheet model years. The coupling is performed after each year of climate model integrations. For easy reference, ice sheet model years in the coupled experiments are ten times the corresponding climate model years, thus climate model year 10 corresponds to ice model years 100 to 109.

Name	Boundary conditions	Coupling	Duration (CM yr)
PI-mPISM	PI	1 : 10	1000
LGM-mPISM	LGM	1 : 10	2999
LGM-mPISM-W	LGM	1 : 10	700
LGM-ICE-5G	LGM	none	649

[Title Page](#)
[Abstract](#)
[Introduction](#)
[Conclusions](#)
[References](#)
[Tables](#)
[Figures](#)

[Back](#)
[Close](#)
[Full Screen / Esc](#)
[Printer-friendly Version](#)
[Interactive Discussion](#)


Coupled ice sheet–climate modeling

F. A. Ziemer et al.

Table 2. Boundary conditions differing between the LGM and pre-industrial setups.

Parameter	LGM	Pre-industrial
Topography	ICE-5G 21ka	ICE-5G 0ka
Eccentricity	0.0190	0.0167
Obliquity	22.95°	23.45°
Angle of Perihelion	294.4°	282.0°
CO ₂ (ppm)	185	280
N ₂ O (ppm)	0.20	0.27
CH ₄ (ppm)	0.35	0.67

Title Page

Abstract

Introduction

Conclusions

References

Tables

Figures



Back

Close

Full Screen / Esc

Printer-friendly Version

Interactive Discussion



Coupled ice sheet–climate modeling

F. A. Ziemer et al.

Table 3. Greenland mass balance. RACMO2, Polar MM5 (PMM5) (Box et al., 2006), and MAR (Fettweis, 2007) data are for the period 1958–2007 (RACMO2, MAR), resp. 1958–2006 (PMM5) and are taken from Supplement S1 from Ettema et al. (2009).

	mPISM	RACMO2	PMM5	MAR
Accumulation (Gtyr^{-1})	766	697	678	578
Ablation (Gtyr^{-1})	271	228	322	290
Accumulation – Ablation (Gtyr^{-1})	495	469	356	288

Title Page

Abstract

Introduction

Conclusions

References

Tables

Figures



Back

Close

Full Screen / Esc

Printer-friendly Version

Interactive Discussion



Coupled ice sheet–climate modeling

F. A. Ziemer et al.

Table 4. Ice sheet volumes and their changes in PI-mPISM averaged over the last 1000 yr of the simulation. Greenland volume: Bamber et al. (2001). Glaciers outside of Greenland and Antarctica are estimated between 0.05 and 0.13 Mio km³ in Lemke et al. (2007).

Ice sheet	Volume (Mio km ³)		Drift (km ³ yr ⁻¹)
	Present day	mPISM	mPISM
Greenland	2.93	3.65	-14
Canada and Alaska		1.2	+38
Siberia		0.94	+86
Arctic Islands		0.14	-0.1
Total		5.9	+106

[Title Page](#)
[Abstract](#)
[Introduction](#)
[Conclusions](#)
[References](#)
[Tables](#)
[Figures](#)
[Back](#)
[Close](#)
[Full Screen / Esc](#)
[Printer-friendly Version](#)
[Interactive Discussion](#)


Coupled ice sheet–climate modeling

F. A. Ziemer et al.

Table 5. Heat budget of the Arctic Ocean in years 1650–2349 of LGM-mPISM and the same years of LGM-mPISM-W (the comparison experiment with cut ice shelf–ocean heat fluxes). The boundary between Arctic Ocean and GIN Sea is drawn at Fram Strait.

Flux	LGM-mPISM	LGM-mPISM-W
Atmosphere–ocean (TW)	–29.4	–38.3
Ice shelf–ocean (TW)	–12.3	0
Sea ice export (mSv)	123	103
Heat export corresponding to sea ice export (TW)	33.4	27.9
Cooling of the ocean water (TW)	8.3	10.3

Title Page

Abstract

Introduction

Conclusions

References

Tables

Figures



Back

Close

Full Screen / Esc

Printer-friendly Version

Interactive Discussion



Coupled ice sheet–climate modeling

F. A. Ziemer et al.

[Title Page](#)

[Abstract](#)

[Introduction](#)

[Conclusions](#)

[References](#)

[Tables](#)

[Figures](#)



[Back](#)

[Close](#)

[Full Screen / Esc](#)

[Printer-friendly Version](#)

[Interactive Discussion](#)



Table 6. LGM Ice sheet volumes and drift. For the time evolution in the model see Fig. 12. For the ICE-5G-reconstruction see Peltier (2004).

Ice sheet	Volume (Mio km ³)		Drift (km ³ yr ⁻¹)
	ICE-5G	mPISM	mPISM
Greenland	4.3	5.8	−2.6
Iceland	0.17	0.28	+1.2
Laurentide	36	31	+28
Siberia	0	9.3	+108
Fennoscandian	8.2	11.6	+156
Total	48.7	60	+233

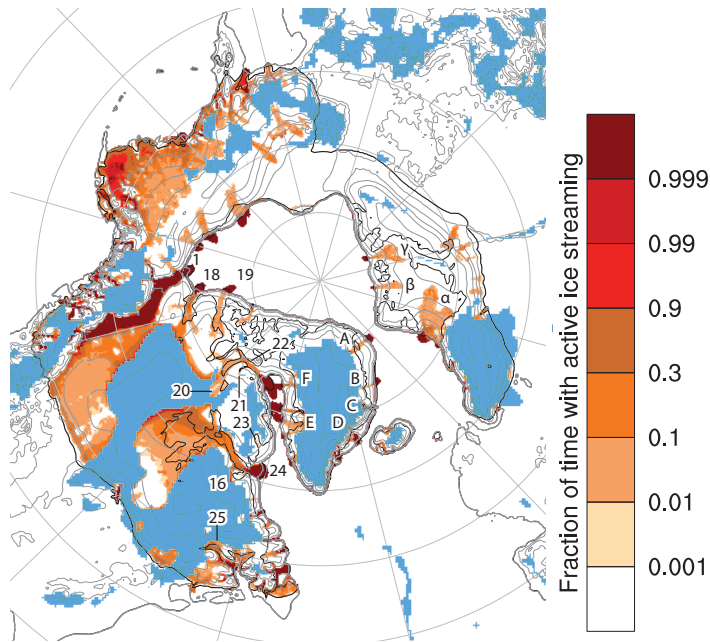


Fig. 1. Ice streams. Brownish/red colors mark the fraction of time that a grid cell is sliding at more than 1 myr^{-1} . Blue marks areas where the ice is not permitted slide due to the lack of sediments in the reconstruction of Laske and Masters (1997). Only the time when the grid cell is ice-covered is taken into consideration, therefore ice shelves are considered as constantly sliding. Numbers match the ice stream numbering in Stokes and Tarasov (2010) and are as follows: (1) Mackenzie, (16) Ungava Bay, (18) Amundsen Gulf, (19) M'Clure Strait, (20) Gulf of Boothia, (21) Admiralty Inlet, (22) Lancaster Sound, (23) Cumberland Sound, (24) Hudson Strait, (25) Laurentian. Letters mark Greenland ice streams: (A) Northeast Greenland Ice Stream, (B) Keeser Franz Joseph Fjord, (C) Scoresby Sund, (D) Kagerdlugssuaq, (E) Jakobshaven Isbrae, (F) Kong Oscar Glacier. Greek letters (α, β, γ) mark Barents Shelf ice streams.

Coupled ice sheet–climate modeling

F. A. Ziemer et al.

[Title Page](#)

[Abstract](#) [Introduction](#)

[Conclusions](#) [References](#)

[Tables](#) [Figures](#)

[◀](#) [▶](#)

[◀](#) [▶](#)

[Back](#) [Close](#)

[Full Screen / Esc](#)

[Printer-friendly Version](#)

[Interactive Discussion](#)



Coupled ice sheet–climate modeling

F. A. Ziemer et al.

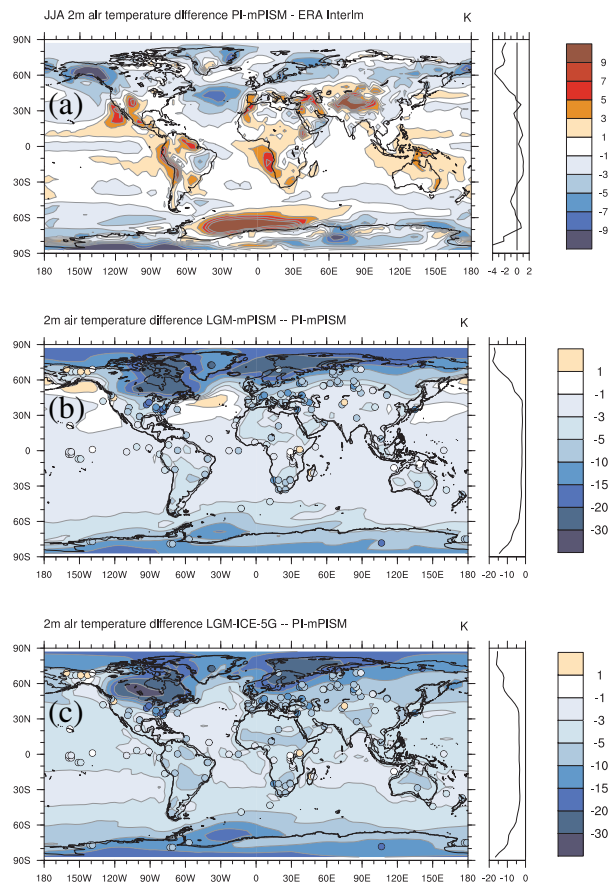


Fig. 2. SAT differences. **(a)** PI-mPISM – ERA INTERIM (June/July/August, JJA), **(b)** LGM-mPISM – PI-mPISM (annual mean), **(c)** LGM-ICE-5G – PI-mPISM (annual mean). Dots show proxy data for LGM – present day from Schmittner et al. (2011) and Kim et al. (2008). The plots on the right of each map show zonal means.

Coupled ice sheet–climate modeling

F. A. Ziemer et al.

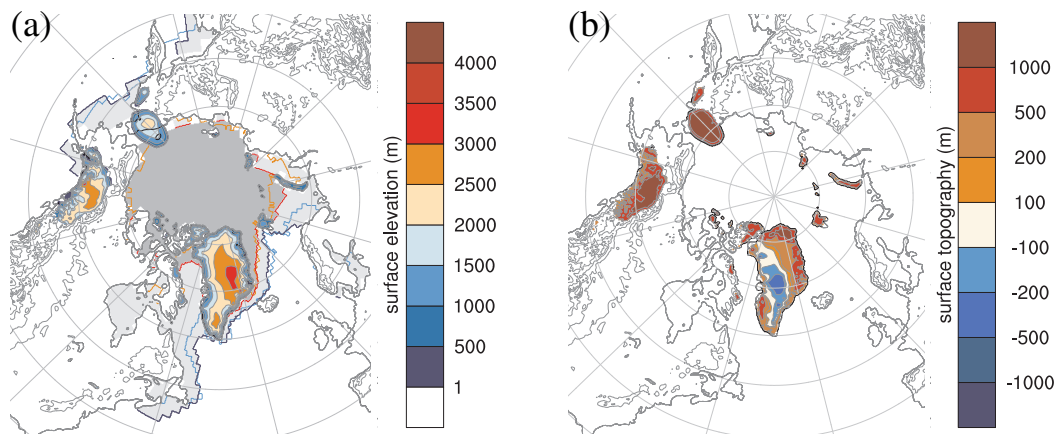


Fig. 3. Ice sheets in PI-mPISM. **(a)** The surface topography in mPISM averaged over the last 1000 ice-model years of PI-mPISM. Isolines are drawn every 500m. Ice covered regions are colored. Over the ocean, dark gray with red outline indicates areas with perennial ice cover (15 % level) in more than 50 % of the model years. Light gray with dark blue-gray outline indicates temporary ice cover in more than 50 % of the model years. The Bering strait appears to be ice-free because it is slightly displaced to the west in the ocean model. The orange outline marks areas which have permanent sea ice cover in more than 50 % of the years 1870 to 2010 according to the HadISST sea ice data set (Rayner et al., 2003), the light blue outline marks areas that have temporary sea ice cover in more than 50 % of these years according to HadISST. **(b)** The difference between the modeled pre-industrial topography and the present day topography (ETOPO1, Amante and Eakins, 2009).

Title Page

Abstract

Introduction

Conclusions

References

Tables

Figures

⏪

⏩

◀

▶

Back

Close

Full Screen / Esc

Printer-friendly Version

Interactive Discussion



Coupled ice sheet–climate modeling

F. A. Ziemer et al.

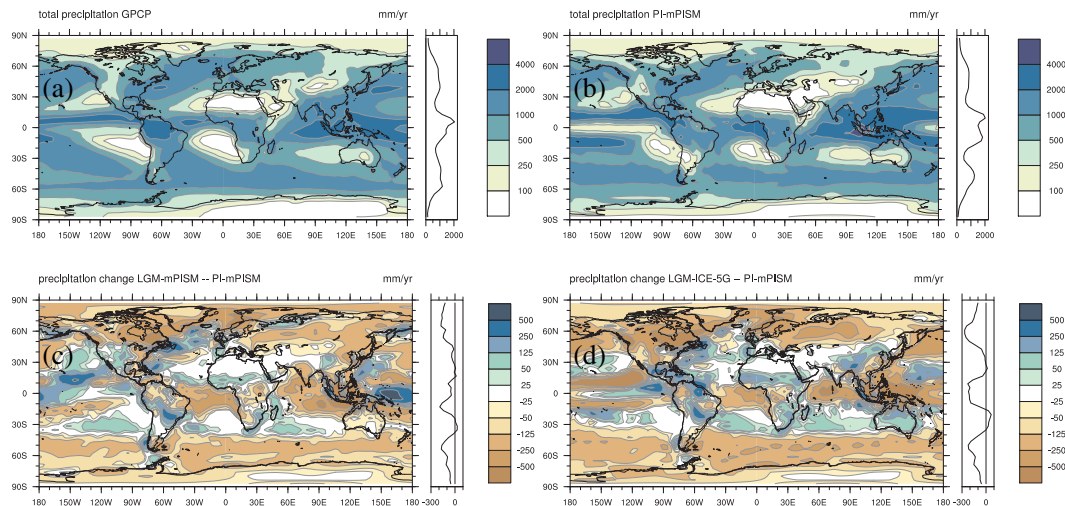


Fig. 4. Measured and modeled precipitation. **(a)** from the GPCP dataset (Adler et al., 2003), **(b)** PI-mPISM, **(c)** LGM-mPISM – PI-mPISM, **(d)** LGM-ICE-5G – PI-mPISM. The plots on the right of each map show zonal means.

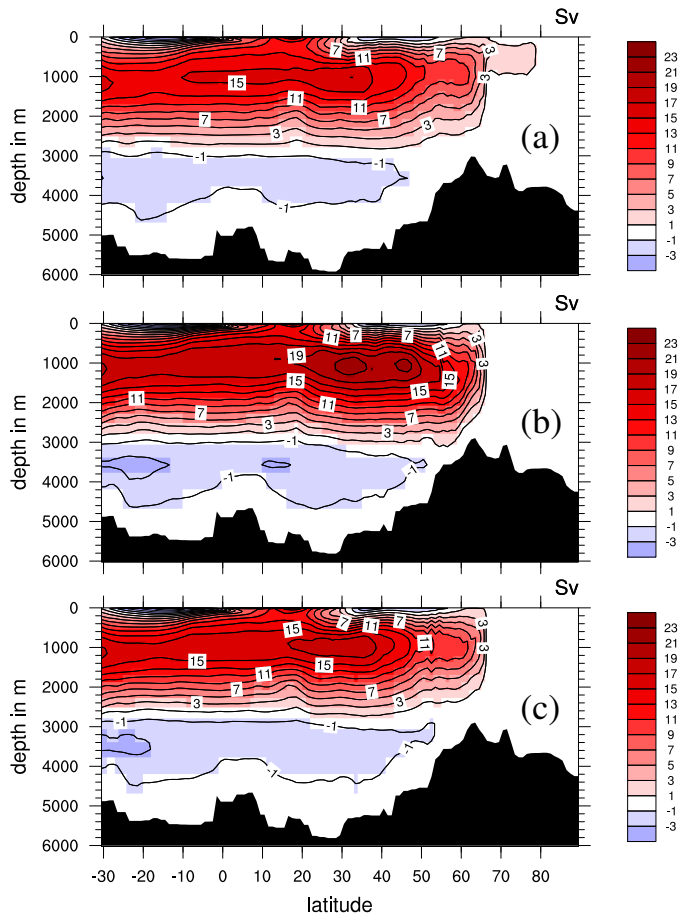


Fig. 5. Atlantic Meridional overturning circulation stream functions for pre-industrial and LGM climate states. **(a)** PI-mPISM, **(b)** LGM-mPISM, **(c)** LGM-ICE-5G. Positive values indicate clockwise flow.

Coupled ice
sheet–climate
modeling

F. A. Ziemer et al.

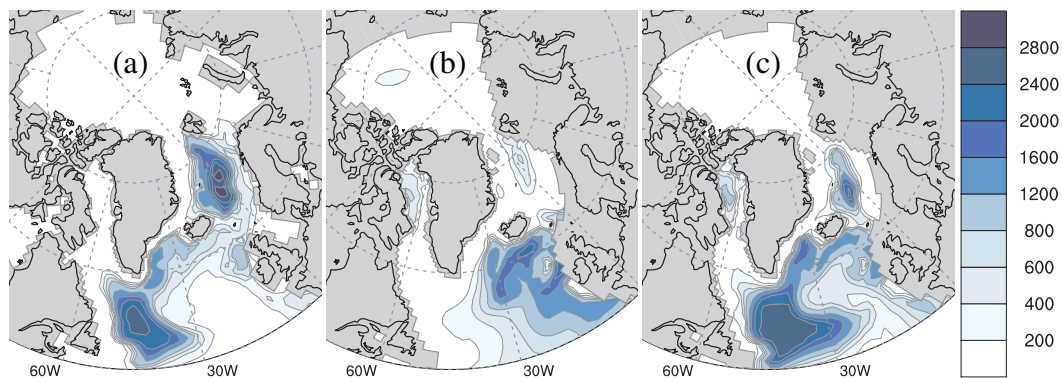


Fig. 6. March mixed layer depth. Long-term mean values are given in meters **(a)** PI-mPISM, **(b)** LGM-mPISM, **(c)** LGM-ICE-5G.

[Title Page](#)[Abstract](#)[Introduction](#)[Conclusions](#)[References](#)[Tables](#)[Figures](#)[⏪](#)[⏩](#)[◀](#)[▶](#)[Back](#)[Close](#)[Full Screen / Esc](#)[Printer-friendly Version](#)[Interactive Discussion](#)

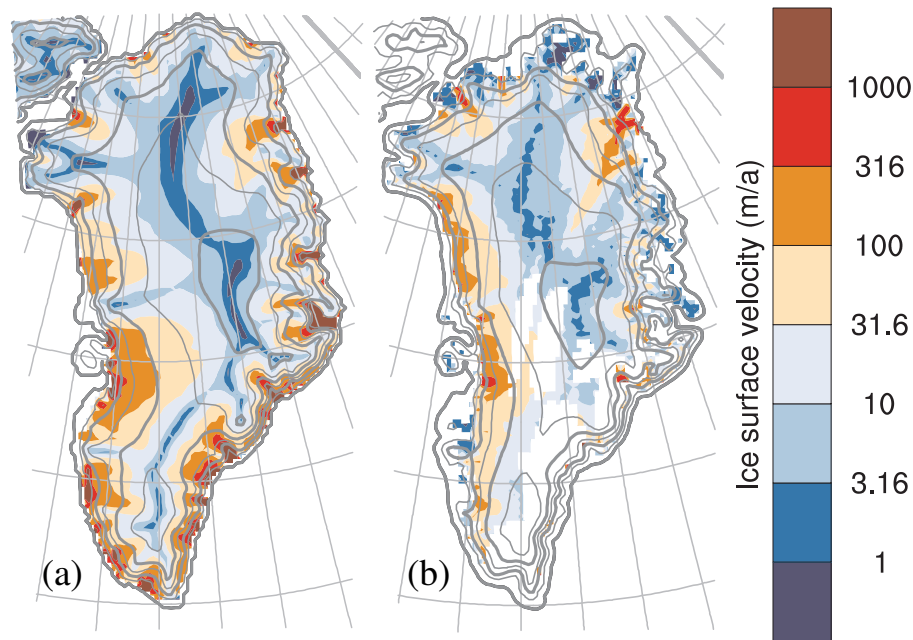


Fig. 7. Greenland Ice Sheet surface velocities. Plotted on a logarithmic color scale. Contour lines show the surface elevation in steps of 500 m with thick lines at multiples of 1000 m. **(a)** modeled velocities from PI-mPISM, **(b)** observed velocities (Joughin et al., 2010b) and smoothed-out ETOPO1 topography (Amante and Eakins, 2009). White areas inside the ice sheet indicate data gaps.

Coupled ice sheet–climate modeling

F. A. Ziemer et al.

Title Page

Abstract Introduction

Conclusions References

Tables Figures

⏪ ⏩

◀ ▶

Back Close

Full Screen / Esc

Printer-friendly Version

Interactive Discussion



Coupled ice sheet–climate modeling

F. A. Ziemer et al.

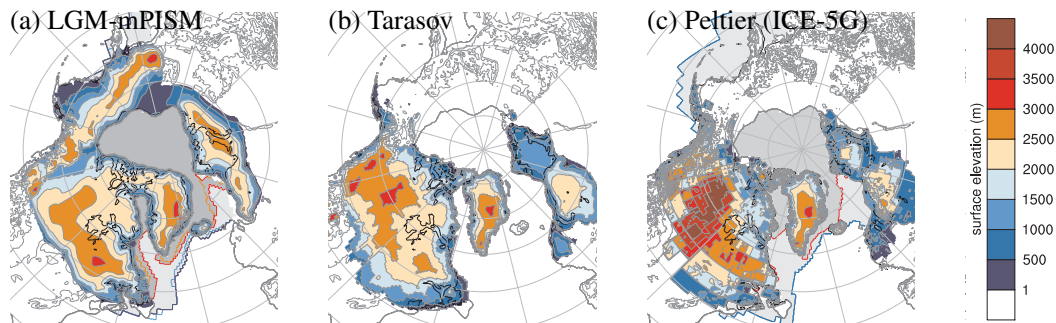


Fig. 8. Surface topography and sea ice. Isolines mark the topography at 500 m intervals. Ice covered regions are colored. Over the ocean, dark gray with red outline indicates areas with perennial ice cover (15 % level) in more than 50 % of the model years. Light gray with blue outline indicates temporary ice cover in more than 50 % of the model years. **(a)** The surface topography in mPISM averaged over the full 30 kyr of LGM-mPISM, yellow/orange lines in the ocean mark perennial ice cover in LGM-mPISM-W, light blue lines mark temporary ice cover in LGM-mPISM-W **(b)** The LGM topography provided by Lev Tarasov. **(c)** The surface topography from the ICE-5G reconstruction of Peltier (2004) and sea ice from LGM-ICE-5G. The corresponding plot for PI-mPISM is shown in Fig. 3a.

Title Page

Abstract

Introduction

Conclusions

References

Tables

Figures

◀

▶

◀

▶

Back

Close

Full Screen / Esc

Printer-friendly Version

Interactive Discussion



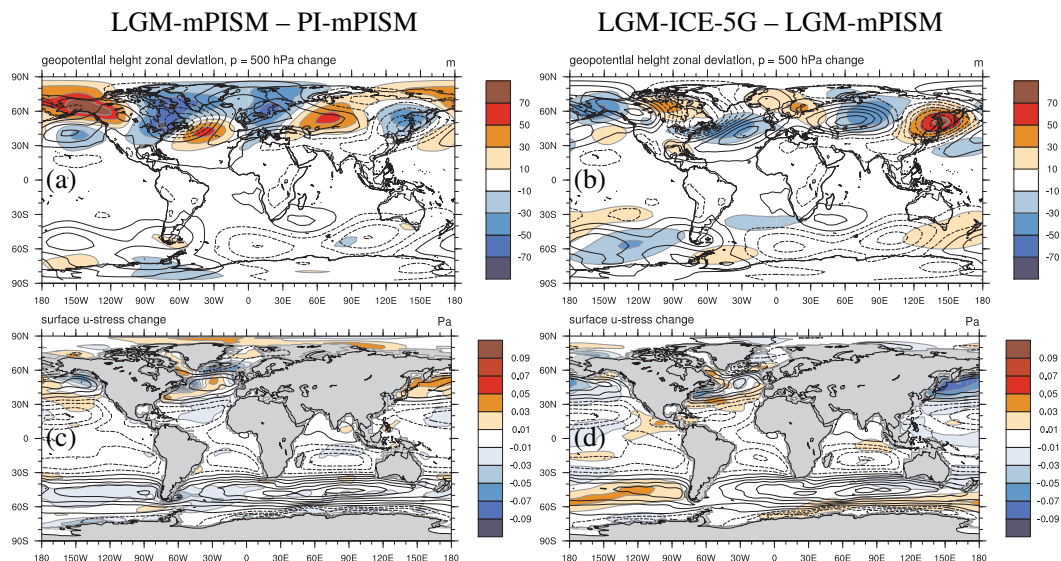


Fig. 9. 500 hPa geopotential height and wind stress.

(a, b) geopotential height, (c, d) zonal wind stress;
 (a, c) LGM-mPISM – PI-mPISM, (b, d) LGM-ICE-5G – LGM-mPISM.

(a, b) Colors show the zonal deviations of the difference in 500 hPa geopotential height. Contour lines show the zonal deviations of 500 hPa geopotential height in (a) PI-mPISM and (b) LGM-mPISM on 20 m levels starting at ± 10 m. Dashed contour lines mark negative values.

(c, d) Colors show the difference in zonal wind stress. Contour lines show the zonal wind stress in (c) PI-mPISM and (d) LGM-mPISM on 0.04 Pa levels starting at ± 0.02 Pa. Solid lines and reddish colors mark eastward wind stress, dashed lines and blueish colors westward wind stress.

Coupled ice sheet–climate modeling

F. A. Ziemer et al.

Title Page

Abstract

Introduction

Conclusions

References

Tables

Figures



Back

Close

Full Screen / Esc

Printer-friendly Version

Interactive Discussion



Coupled ice sheet–climate modeling

F. A. Ziemer et al.

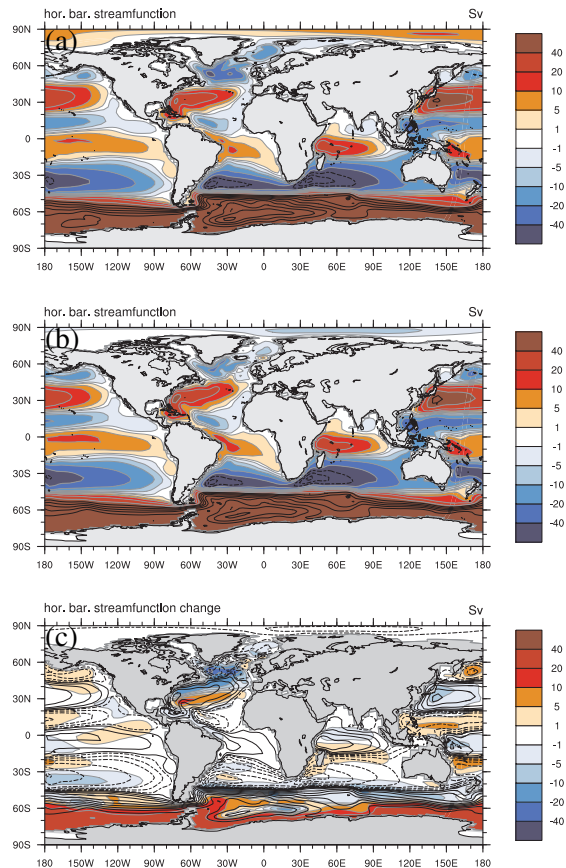


Fig. 10. Barotropic stream function. Positive values indicate clockwise flow. **(a)** PI-mPISM, **(b)** LGM-mPISM, **(c)** LGM-ICE-5G – LGM-mPISM **(a, b)** For values beyond ± 40 Sv, black contour lines are drawn at multiples of 20 Sv. **(c)** black contour lines show the circulation in LGM-mPISM at levels of $\pm 1, 5, 10, 20, 40, 60, \dots$ Sv. Dashed contour lines mark negative values.

**Coupled ice
sheet–climate
modeling**

F. A. Ziemer et al.

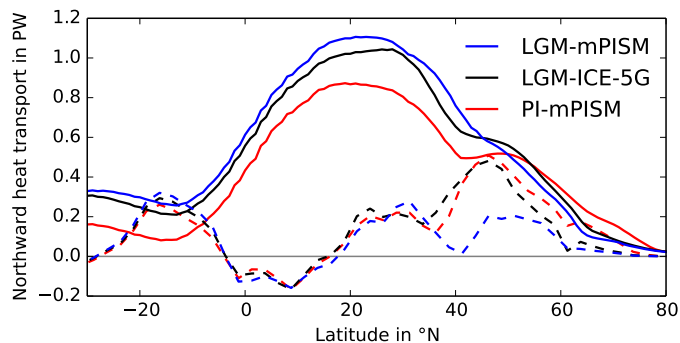


Fig. 11. Atlantic Ocean heat transports. Solid lines mark the total heat transport, dashed lines the gyre contribution. The difference is the AMOC contribution.

[Title Page](#)[Abstract](#)[Introduction](#)[Conclusions](#)[References](#)[Tables](#)[Figures](#)[⏪](#)[⏩](#)[◀](#)[▶](#)[Back](#)[Close](#)[Full Screen / Esc](#)[Printer-friendly Version](#)[Interactive Discussion](#)

Coupled ice sheet–climate modeling

F. A. Ziemer et al.

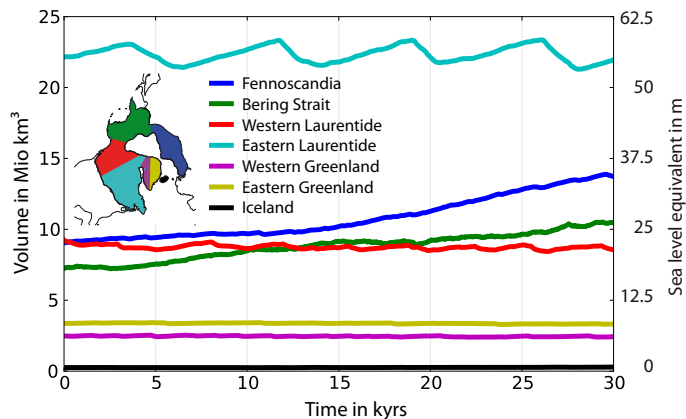


Fig. 12. Development of the ice sheet volumes in LGM-mPISM. The inset shows the split of the ice sheets into different regions for the diagnosis.

Title Page

Abstract

Introduction

Conclusions

References

Tables

Figures

⏪

⏩

◀

▶

Back

Close

Full Screen / Esc

Printer-friendly Version

Interactive Discussion

